JVI Accepted Manuscript Posted Online 20 March 2019
J. Virol. doi:10.1128/JVI.02205-18

Chicken organic anion transporting polypeptide 1A2, a novel avian hepatitis E virus (HEV) ORF2-interacting protein, is involved in avian HEV infection

Huixia Li[1], Mengnan Fan[1], Baoyuan Liu[1], Pinpin Ji[1], Yiyang Chen[1], Beibei Zhang[1], Yani Sun[1], Baicheng Huang[1], Yuchen Nan[1], Zhenzhao Sun[2], James P. Stewart[3], Julian A. Hiscox[3], Qin Zhao[1#], En-Min Zhou[1#]

[1]Department of Preventive Veterinary Medicine, College of Veterinary Medicine, Northwest A&F University, Yangling, Shaanxi, China; [2]Harbin Veterinary Research Institute, Chinese Academy of Agricultural Science, Harbin, China; [3]Department of Infection Biology, Institute of Infection and Global Health, University of Liverpool, Liverpool, UK

[#] **Corresponding authors:**

Dr. Qin Zhao

Tel. 86-29-87091117

E-mail. qinzhao_2004@nwsuaf.edu.cn

Prof. En-Min Zhou

Tel. 86-29-87091117

E-mail. zhouem@nwsuaf.edu.cn

Running title: OATP1A2 involved in avian HEV infection

Number of words in abstract: 213

Number of words in text: 8155

ABSTRACT

Avian hepatitis E virus (HEV) is the main causative agent of big liver and spleen disease in chickens. Due to the absence of a highly effective cell culture system, there are few reports about the interaction between avian HEV and host cells. In this study, organic anion transporting polypeptide 1A2 (OATP1A2) from the chicken liver cells was identified to interact with ap237, a truncated avian HEV capsid protein spanning amino acids 313 to 549, by the GST pull-down assay. Then, the GST pull-down and indirect ELISA assays further confirmed that the extracellular domain of OATP1A2 directly binds with ap237. The expression levels of OATP1A2 in host cells are positively correlated with the amounts of ap237 attachment and virus infection. The distribution of OATP1A2 in different tissues is consistent with avian HEV infection *in vivo*. Finally, when the functions of OATP1A2 in the cells are inhibited by its substrates, an inhibitor or blocked by ap237 or anti-OATP1A2 sera, the attachment and infection of avian HEV of the host cells is significantly reduced. Collectively, these results displayed that for the first time, OATP1A2 interacts with the avian HEV capsid protein and can influence viral infection in host cells. The present study provided new insight to understand the process of avian HEV infection of host cells.

IMPORTANCE

The process of viral infection is centered around the interaction between the virus and host cells. Due to the lack of a highly effective cell culture system *in vitro*, there is little understanding about the interaction between avian HEV and its host cells. In this study, a total of seven host proteins were screened from chicken liver cells by a truncated avian HEV capsid protein (ap237) in which the host protein OATP1A2 interacted with ap237. Overexpression of OATP1A2 in LMH cells can promote ap237 adsorption as well as avian HEV adsorption and infection of LMH cells. When the function of OATP1A2 in the cells was inhibited by substrates or inhibitors, the attachment and infection of avian HEV significantly decreased. The distribution of OATP1A2 in different chicken tissues corresponded with the tissues of avian HEV infection. This is the first finding that OATP1A2 is involved in viral infection of host cells.

INTRODUCTION

Hepatitis E virus (HEV) belongs to the *Hepeviridae* family which contains genera *Orthohepevirus* and *Piscihepevirus* (1). All four major HEV genotypes that infect humans and genotypes 5 and 6 isolated from wild boar and genotypes 7 and 8 from camels are assigned to the species *Orthohepevirus* A. Avian HEV, the second known animal strain of HEV, belongs to the species *Orthohepevirus* B (1, 2). It was identified from chickens with big liver and spleen disease, also known as hepatitis-splenomegaly syndrome (3), which can cause slightly increased mortality (1%-4%) and decreased egg production (10%-40%) in broiler breeders and laying hens aged 30 to 72 weeks (4-6). In addition, avian HEV RNA has also been detected in healthy chickens (7). To date, both the fecal-oral transmission route and vertical transmission of avian HEV have been demonstrated (8, 9).

Until now, five genotypes (genotypes 1 to 5) and a single serotype of avian HEV from chickens have been identified (10-15). The avian HEV genome is a positive (+)-sense single-stranded RNA of approximately 6.6 kb, which consists of three open reading frames (ORFs): ORF1, ORF2, and ORF3 (16). Out of these, ORF2 encodes the virus capsid protein, including 606 amino acids (16). Some previous studies indicated that the capsid protein is closely related with viral infection of the host cell and induction of the immune response (17-21). Over the last decade, the major focus of research was on the antigen properties of the capsid protein (18-20, 22), but less effort has been directed towards its function in virus infection.

In regard to human HEV, it was documented that the truncated ORF2 protein named p239 (amino acids 368–606), a self-assembling virus-like particle that covers the complete P domain (23), can bind to HepG2 cells and serve as a material replacing the natural viral particle to research the interaction between the virus and host cells (24). Then, utilizing p239 as a bait protein, the host factors GRP78/Bip, α-tubulin, heat shock protein 90 (HSP90),

77 cytochrome P4502C8, and retinol-binding protein 4 were screened and specifically interacted
78 with the HEV ORF2 protein (25, 26). In addition, using another truncated ORF2 protein
79 expressed in insect cells as a bait protein (amino acids 112-606), several membrane proteins,
80 such as heparin surface proteoglycans (27), asialoglycoproteins ASGR1 and ASGR2 (28),
81 and transmembrane protein 134 (29), were identified. The functions of these host factors in
82 virus infection are different. For example, both heparin surface proteoglycans and
83 asialoglycoproteins mainly mediate viral binding and entry, while transmembrane protein 134
84 (located in the endoplasmic reticulum) negatively regulates ORF2-mediated inhibition of the
85 NF-κB signaling pathway.

86 In this study, based on the alignments of the amino acids (aa) between human and avian
87 HEV ORF2 proteins, the aa 313-549 region of the avian HEV ORF2 protein (named ap237)
88 was selected as the bait protein. This region corresponded with the aa region of the human
89 HEV p239 protein. In some previous studies, the results showed that ap237 contains most of
90 the antigenic epitopes of avian HEV (18-20) and the key domain (aa 471-507) for binding to
91 the LMH cell (30) derived from chicken hepatocellular carcinoma epithelial cells (31) that
92 support avian HEV replication (32). Then, ap237 was employed as a bait protein to target the
93 host factors in chicken liver tissue. A total of seven host proteins were pulled from chicken
94 liver cells by ap237, and out of these host proteins, the organic anion transporting
95 polypeptide 1A2 (OATP1A2), a multiple transmembrane protein localizing on the cell
96 membrane and expressed in the liver, was chosen for subsequent research. Firstly, the direct
97 binding between ap237 and the ectodomain of OATP1A2 was determined. Following this, the
98 functions of OATP1A2 during avian HEV attachment and infection were analyzed using
99 LMH cell line lacking endogenous OATP1A2 and LMH cells stably expressing OATP1A2.
100 Finally, the correlations of OATP1A2 expression and avian HEV infection in different tissues
101 were determined. The results of the present study indicate that OATP1A2 is a cofactor

102 involved in avian HEV infection of the host cells.

103

RESULTS

Design, expression, and purification of GST-ap237. In a previous study, it was documented that the aa 368-606 region of the human HEV ORF2 protein (named p239) was expressed by a bacterial system and can form polymers (33). p239 can enter into the host cells by mimicking the natural HEV particle (24). Through the alignment of human and avian HEV ORF2 amino acids, it was observed that the aa 313-549 region of the avian HEV ORF2 protein corresponded to the p239 region of the human HEV ORF2 protein, and this region was selected (Fig. 1A). In addition, the 3D modeling of the avian HEV ORF2 protein showed that ap237 consisted of part of a middle (M, aa 313-400) and a complete protruding (P, aa 401-549) domain (Fig. 1B), which was predicted based on the 3D structure of the human capsid protein (23).

According to the above alignments and prediction, ap237 with N-terminal GST-tag was designed and expressed as a bait protein for the GST pull-down assay. The soluble recombinant protein GST-ap237 (55 kDa) was successfully expressed in the supernatant of the cell lysate (Fig. 1C) and purified using the Glutathione Sepharose 4 Fast Flow (Fig. 1C). Western blot analysis revealed that GST-ap237 was bound with both anti-GST antibodies (Fig. 1D) and the 3E8 mAb specific to ap237 (Fig. 1E).

Screening host proteins specifically pulled by ap237. To identify cellular proteins from chicken liver cells that interact with ap237, the GST pull-down assay and mass spectrometry (MS) were performed. The silver staining results of SDS-PAGE showed that there were at least five specific bands in GST-ap237 lanes that were not observed in the lanes with only GST (Fig. 2A). These five bands were cut and mixed together to analyze via MS. The MS results showed that 7 proteins were identified (Table 1). Out of these seven, A0A1D5PMA0 (Solute carrier organic anion transporter family member 1A2, OATP1A2) was predicted as a

128 cell membrane protein, while the other proteins were located in cytoplasm or nucleus. To
129 confirm the cellular location of OATP1A2, primary cultured chicken embryo hepatocytes
130 (CEH) were probed with anti-GST-1A2^{ecto} mouse sera and detected using confocal
131 immunofluorescence and Western blot assays. The results showed that the OATP1A2 mainly
132 located in the cell membrane (Fig. 2B and 2C).

133 **OATP1A2 interaction and co-localization with ap237.** Upon review of MS results of
134 the silver stained bands and MS results of the protein complex, one of the host proteins, a
135 membrane protein, OATP1A2, was screened. In human, OATP1A2 is a transmembrane
136 transporter and expressed on the cell membrane in liver (34). It is well known that the
137 chicken liver is the major tissue targeted by avian HEV infection (9), so OATP1A2 was
138 selected for this study. Firstly, to further confirm ap237 interaction with OATP1A2, the Co-IP
139 assay was performed by transient co-expression of OATP1A2-3Flag and HA-ap237 in HEK
140 293T cells. The results showed that OATP1A2-3Flag can be pulled by HA-ap237 using anti-
141 HA mAb but not with HA-ORF3 (Fig. 3A). In turn, HA-ap237, not HA-ORF3, can also be
142 pulled by OATP1A2-3Flag using anti-Flag mAb (Fig. 3B). In addition, to examine the
143 localization of ap237 and OATP1A2 in the cells, HEK 293T cells were transiently co-
144 transfected with plasmids as above. After 48 hours of transfection, the subcellular localization
145 of OATP1A2-3Flag and HA-ap237 was examined by confocal microscopy. Both of the two
146 proteins were distributed throughout the cytoplasm, and OATP1A2 co-localized extensively
147 with the ap237 protein with Manders' overlap coefficient of 0.89 (Fig. 3C).

148 **OATP1A2 ectodomain direct binding with ap237.** To identify the part of OATP1A2
149 directly interacting with ap237, OATP1A2 and ap237 without any tags were separately
150 expressed by a bacterial system. For OATP1A2, the results showed that the protein was a
151 multi-transmembrane protein with 9 transmembrane domains, as predicted (Fig. 4).
152 Meanwhile, the 3D structure of OATP1A2 from chickens was predicted based on the d1pw4a

template with a confidence of 100% and coverage of 66%; this also exhibited the transmembrane structure (Fig. 5A). Then, the direct interaction of $1A2^{ecto}$ (the ectodomain of OATP1A2) and ap237 was determined by the GST pull-down assay and indirect ELISA assay. Firstly, using the bacterial system, $1A2^{ecto}$ with an N-terminal GST-tag was successfully expressed as a soluble form as shown in SDS-PAGE (Fig. 5B, left) and reacted with anti-GST antibodies, as demonstrated by Western blot (Fig. 5B, right); ap237 without any tag was also successfully expressed by a bacterial system (Fig. 5C). Under non-denature conditions, a part of the protein formed a multimeric structure. Then, by the GST pull-down assay, Western blot analysis showed that ap237 was pulled by GST-$1A2^{ecto}$ as the bait protein, but no pulling of ap237 was observed with only GST (Fig. 5D). Furthermore, the sp239 control protein from swine HEV was not pulled by GST-$1A2^{ecto}$. In addition to the GST pull-down assay, indirect ELISA was also used to confirm the $1A2^{ecto}$ direct binding with ap237. The OD_{450nm} values revealed that GST-$1A2^{ecto}$ can bind in a specific and dose-dependent manner with ap237 at a GST-$1A2^{ecto}$ concentration of 20 μg/mL, but this does not occur with GST protein (Fig. 5E). Meanwhile, indirect ELISA results also indicated that chicken OATP1A2 (GST-$1A2^{ecto}$) specifically binds with ap237, but not with other capsid proteins from mammalian HEVs, namely, sp239, r239, sar239, ker239, and PRRSV N protein (Fig. 5F). Furthermore, chicken OATP1A2 (GST-$1A2^{ecto}$) also specifically binds with the soluble capsid proteins in avian HEV infected sera (Fig. 5F).

$LMH^{1A2\text{-}GFP}$ cell lines with stable expression of OATP1A2 and knockdown treatment. To investigate the relationship of OATP1A2 with ap237 *in vitro*, the $LMH^{1A2\text{-}GFP}$ cell line with stable expression of OATP1A2 fused with GFP protein was generated by lentivirus infection. The LMH^{GFP} cell line only expressing GFP protein was also generated for the control. The green fluorescence from the GFP protein in $LMH^{1A2\text{-}GFP}$ cells was observed under a fluorescence microscope (Fig. 6A, left), and the expression of OATP1A2-

178 GFP was also detected by anti-GST-1A2^{etco} sera with red fluorescence (Fig. 6A, right). In
179 addition, qPCR showed that the relative mRNA level of OATP1A2 in LMH$^{1A2\text{-}GFP}$ cells was
180 significantly ($P < 0.001$) higher than that in LMH cells, LMH^{GFP} cells, DF-1 cells, and CEH
181 (Fig. 6B). Western blot analysis further showed that the OATP1A2 fused with GFP protein
182 was mainly expressed in solubilized membrane and membrane-associated proteins (SMPs
183 and MAPs) and membrane fractions (MFs), as well as in a small amounts in the cytoplasm
184 (Cytos) (Fig. 6C).

185 To knockdown the expression of OATP1A2 in the LMH$^{1A2\text{-}GFP}$ cells, three small
186 interfering RNAs (si1A2-1, si1A2-2, and si1A2-3) targeting the mRNA encoding OATP1A2
187 were transfected into the cells. All three small interfering RNAs (siRNAs) effectively ($P <$
188 0.001) knocked down the expression of OATP1A2 mRNA and protein in LMH$^{1A2\text{-}GFP}$ cells, at
189 a concentration of 50 nM (Fig. 6D). Comparing the OATP1A2 expression levels in the
190 LMH$^{1A2\text{-}GFP}$ cells by the three siRNAs interference, the si1A2-1 was selected for the
191 following experiments (Fig. 6D) since OATP1A2 mRNA was significantly decreased in the
192 varying concentrations of si1A2-1 (10 nM, 20 nM, 30 nM, 50 nM, and 100 nM; Fig. 6E,
193 upper). Western blot showed that, except for a small amount expression at 10 nM, OATP1A2
194 was not detected in the other concentrations in LMH$^{1A2\text{-}GFP}$ cells (Fig. 6E, below).

195 **OATP1A2 enhances ap237 attachment to LMH cells.** A previous study showed that
196 ap237 can mimic natural avian HEV to attach to host cells (30). In this study, ap237 was used
197 to analyze the relationship between ap237 attachment and the expression of OATP1A2 in
198 cells. The Western blot results showed that the amount of ap237 binding with LMH$^{1A2\text{-}GFP}$
199 cells transfected with control siRNA (siNCtrl) were significantly higher than that with LMH
200 and LMH^{GFP} cells (Fig. 7A) which had the similar amounts of bound ap237. Meanwhile,
201 when the expression levels of OATP1A2 in the LMH$^{1A2\text{-}GFP}$ cells were reduced by the si1A2-
202 1 (50 nM) interference, the amount of ap237 attachment to these cells markedly decreased

(Fig. 7A). Additionally, the flow cytometry assay revealed that ap237 attached to 17.2% of LMH^{GFP} cells and 59.8% of LMH$^{1A2\text{-}GFP}$ cells, which is a significant increase. Furthermore, ap237 attachment decreased (34.3%) in LMH$^{1A2\text{-}GFP}$ cells transfected with si1A2-1 (Fig. 7B). Collectively, the Western blot and flow cytometry results both suggested that high expression levels of OATP1A2 in the cells enhance ap237 attachment.

OATP1A2 enhances avian HEV attachment and infection of LMH cells. To determine avian HEV infection in the LMH$^{1A2\text{-}GFP}$ cells, the presence of replicative intermediates of avian HEV RNA in the cells were detected by negative-strand-specific RT-PCR and avian HEV load in the cell lysates over time were detected by TaqMan real-time RT-PCR. CEH were used as positive control. The results showed that in CEH and LMH$^{1A2\text{-}GFP}$ cells the negative strands of CaHEV were detected starting on 2 days post-infection, while in LMH and LMH^{GFP} cells they were detected starting on 4 days post-infection (Fig. 8A). The quantification of viral ORF3 RNA revealed that the CaHEV loads increased over time from all four cells and the ORF3 RNA copies in LMH$^{1A2\text{-}GFP}$ cells were significantly higher than that from other three cells (Fig. 8A), which was correlated with the expression levels of OATP1A2 RNAs in these cells (Fig. 6B). These results indicated that CaHEV can effectively replicate and propagate in LMH $^{1A2\text{-}GFP}$ cells.

To clarify the relationship between OATP1A2 expression levels and natural avian HEV infection, viral attachment and infection assays in the differently treated cell lines (LMH, LMH^{GFP}, LMH$^{1A2\text{-}GFP}$, and LMH$^{1A2\text{-}GFP}$ transfected with si1A2-1) were performed *in vitro*. Firstly, the amount of CaHEV attachment and infection of LMH$^{1A2\text{-}GFP}$ cells was markedly ($P < 0.001$) higher than when compared with the amount in LMH and LMH^{GFP} cells (Fig. 8B and 8C). Secondly, when the different concentrations (10 nM, 20 nM, 30 nM, 50 nM, and 100 nM) of si1A2-1 targeting OATP1A2 were used to knockdown the expression levels of OATP1A2 as shown in Fig. 6E, the amount of CaHEV attachment and infection of these cells

228 were significantly decreased (Fig. 8B and 8C). In the cells transfected with the siNCtrl,
229 OATP1A2 expression and viral attachment and infection had no significant change ($P > 0.05$;
230 Fig. 8B and 8C).

231 **Inhibition of OATP1A2 reduces avian HEV attachment and infection of LMH cells.**
232 OATP1A2 is an important member of the OATP transporter family and participates in the
233 absorption and transportation of drugs (e.g., imatinib) and some endogenous substrates (e.g.,
234 CDCA and SC). To explore whether or not the substrates or inhibitor of OATP1A2 could
235 specifically inhibit CaHEV attachment and infection in $LMH^{1A2\text{-}GFP}$ cells, the $LMH^{1A2\text{-}GFP}$
236 cells were pre-incubated with the substrates CDCA, SC, and imatinib, or the inhibitor,
237 carvedilol, before CaHEV inoculation. Firstly, the cytotoxicity of these reagents to LMH
238 cells was determined by separately treating the cells with different concentrations of the
239 reagents (data not shown). The results showed that the maximum working concentrations of
240 CDCA, SC, imatinib, and carvedilol were 50 μM, 50 μM, 10 μM, and 10 μM, respectively
241 (Fig. 9A). Under the maximum concentration of the substrates and the inhibitor, the
242 expression of OATP1A2 at both the mRNA and protein levels was significantly decreased to
243 varying extents (Fig. 9B). In the CaHEV attachment and infection assay, the amount of
244 CaHEV ORF3 RNA significantly ($P < 0.05$) decreased in the $LMH^{1A2\text{-}GFP}$ cells pre-incubated
245 with CDCA, SC, carvedilol, and imatinib at the maximum concentrations, and these
246 inhibitions were dose-dependent according to the concentration of the substrates (Fig. 9C).

247 Additionally, in the OATP1A2 blocking assay, ap237 was used as the blocking agent and
248 blocked CaHEV attachment and infection of $LMH^{1A2\text{-}GFP}$ cells in a dose-dependent manner
249 when compared to the control protein, sp239 (Fig. 9D). When anti-GST-$1A2^{etco}$ mouse sera
250 were used as a blocking agent, the results also showed that CaHEV attachment and infection
251 of the cells was blocked when the sera were diluted to 1:5 and 1:50 (Fig. 9E). Moreover, the
252 CaHEV infection of CEH was significantly inhibited by imatinib, ap237, and mouse anti-

GST-1A2^{etco} sera when compared to the corresponding control reagents (Fig. 9F).

Correlation of OATP1A2 expression and avian HEV infection *in vivo*. To define the distribution of OATP1A2 in different tissues from the chickens inoculated with CaHEV, the OATP1A2 protein was detected by an immunohistochemistry (IHC) assay using mouse anti-GST-1A2^{ecto} serum along with PBS and negative mouse serum. The positive immunoreactive signals were detected in chicken tissues of liver, brain, spinal cord, kidney, and testis. As shown in Fig. 10A, the chicken liver, the positive signal of OATP1A2 can be seen in cholangiocytes and Kupffer cells (c and f). In the spinal cord, OATP1A2 expression was observed in axons in white matter (i) and nerve cell bodies in gray matter (l). In the chicken brain, OATP1A2 was almost exclusively expressed in brain capillary cells (o). The localization of OATP1A2 expression in the chicken kidney appeared to be in the apical domain of distal nephrons (r). A significant expression of OATP1A2 had also been detected in spermatocytes in the chicken testis (u).

In addition, to evaluate the agreement of the expression levels of OATP1A2 and CaHEV infection in these chicken tissues, qPCR and Taqman real-time RT-PCR were performed. Firstly, the CaHEV positive strand RNA was detected in the fecal samples of chickens (Fig. 10C), indicating that the chickens were successfully infected by CaHEV. The mRNA of OATP1A2 showed that the relative amounts in the liver, pancreas, bile duct, testis, kidney, brain, and spinal cord were higher than the ones in the crops, glandular stomach, muscle stomach, duodenum, jejunum, ileum, cecum, rectum, lung, spleen, ovary, thymus, and nerve tissue (Fig. 10B). Meanwhile, in regard to CaHEV RNA, the results showed that the amount of viral RNA was also higher in the liver, kidney, testis, brain, and spinal cord than in the crops, jejunum, rectum, and heart (Fig. 10C). In the tissues positive for positive-strand CaHEV ORF3 RNA, except from crop, heart, and muscle, all other tissues were all positive for the negative-strand CaHEV ORF3 RNA. Comparison of the above results implied that the

278 expression of OATP1A2 may also be associated with avian HEV infection *in vivo*.

279 **DISCUSSION**

280 Due to the lack of an efficient cell culture system and animal model, there are few
281 studies about the interaction of HEV with host cells. However, for human HEV, the capsid
282 protein expressed by different systems as the bait protein was used to screen the interaction
283 with host proteins (25, 27-29). For example, p239, a truncated human HEV capsid protein,
284 can form polymers and was used as the bait protein to research the interactions of HEV with
285 host cells (25, 27-29). Following these previous studies about human HEV, ap237 (a
286 truncated capsid protein of CaHEV that corresponds to the aa region of human HEV p239)
287 was designed and used as a bait protein to screen the interaction with host proteins from
288 chicken liver cells by the GST pull-down assay in this study.

289 Among the screened cellular proteins, OATP1A2 (a multiple transmembrane protein
290 localizing on the cell membrane) is a member of an important superfamily of solute carriers
291 which is highly expressed in liver tissue based on the research of human OATP1A2 (34). In
292 present study, OATP1A2 was mainly localized in the cell membrane preparations from CEH
293 and $LMH^{1A2\text{-}GFP}$ cells which contains endogenous OATP1A2 and are stably expressing
294 OATP1A2 protein (Fig. 2C and Fig. 6C). The interaction between ap237 and OATP1A2
295 proteins was determined in HEK 293T cells (Fig. 3C) and the co-localization of OATP1A2
296 with ap237 was seen in the cytoplasm rather than the membrane, which may because of the
297 transient expression of these proteins in the cytoplasm. Furthermore, this protein is involved
298 in the biological transportation of endogenous substrates, including bile acid and bile salt,
299 among others (35, 36). In regard to avian HEV, some previous studies suggested that chicken
300 liver is the main target tissue upon viral infection (4, 37) and bile samples of infected
301 chickens contain high amounts of viral RNA copies (38). Based on these previous findings, it

was speculated that OATP1A2 may have some relationship with avian HEV infection. Following this, the host protein OATP1A2 was selected for research in the present study. The results of Co-IP and indirect ELISA confirmed that the extracellular region of OATP1A2 directly interacts with the avian HEV capsid protein and high expression of OATP1A2 in LMH cells can enhance avian HEV attachment and infection. It was also observed that the expression levels of OATP1A2 in different chicken tissues exhibit a positive correlation with the amount of avian HEV RNA. These results confirmed our speculation that OATP1A2 is involved in avian HEV infection of the host cells. To our knowledge, this is the first time it was reported that OATP1A2 is involved in a viral infection.

Heparin surface proteoglycans and asialoglycoproteins are involved in and facilitate HEV infection by binding to ORF2 (27, 28). To date, no cell specific receptor mediating HEV entry has been identified. Usually, the attachment factors and receptors are often hard to be classified in practice because both of them contribute to effective infection. To invade target cells, many viruses use more than one attachment factor and receptor. As a typical example, Hepatitis C virus utilizes more than 10 molecules for cell entry (39). In present study, the fact that the substrates and inhibitor of OATP1A2, ap237, si1A2, and anti-1A2 sera could not completely block avian HEV infection of cells (Fig. 9), suggesting that OATP1A2 is not an only essential factor for avian HEV infection. More research is necessary to determine the exact role OATP1A2 plays in avian HEV infection.

It is noted that the SLCO1A2 gene (encoding the OATP1A2 protein) is conserved in chickens, humans, chimpanzees, cows, and mice, among others, in the GenBank database (40), but the sequences of OATP1A2 are diverse among different species. We found that the OATP1A2 protein of chickens only shared about 50% aa identities with human OATP1A2 in the Uniprot database. In this study, the results of the indirect ELISA assay also showed that

OATP1A2 can specifically bind with the avian HEV capsid protein, but not with the human, pig, or rabbit HEV capsid proteins. Thus, further experiments are necessary to determine whether the OATP1A2 of different species binds with their respective HEV capsid protein. Further, if they interact among different species, another area of research would be to understand if the binding of OATP1A2 is a result of species tropism or a cross-species infection of HEV. In human HEV, soluble ORF2 proteins circulate in HEV infected patients and are the major antigens in patient sera (41-43). In the present study, the positive reaction of OATP1A2 with avian HEV positive sera (Fig. 5F) indicates that soluble avian HEV ORF2 proteins also exist in avian HEV infected chicken sera and the OATP1A2 interacts with the natural ORF2s.

In the present study, IHC results showed that the distributions of chicken OATP1A2 in chicken tissues are consistent with that of human OATP1A2 in human tissues (34, 44, 45). For human HEV, some previous studies have documented that HEV infection favors Kupffer cells, cholangiocytes, and interstitial lymphocytes in the liver; the cytoplasm of neurons in the gray matter; and the perivascular area in the white matter of the spinal cord and the perivascular area in the brain (46). These results indicate that the distribution of OATP1A2 in human cells correlate with the human cells that are targeted by HEV. Moreover, the results of the present study also confirmed that the distribution of chicken OATP1A2 in different tissues is most consistent with tissues that avian HEV infects. However, the negative and positive RNA of avian HEV were also detected in the tissues not expressing OATP1A2, such as jejunum, ileum, and rectum, which may be explained as that the transmembrane protein OATP1A2 is not only one attachment factors or receptors for avian HEV infection and therefore further studies are needed to elucidate the OATP1A2 functions and identify other factors required for avian HEV infection.

350 Substrates and inhibitors of OATP1A2 can significantly reduce CaHEV attachment and
351 infection of LMH$^{1A2\text{-}GFP}$. One possibility is that the substrates or inhibitors reduce the
352 expression of OATP1A2 (e.g., imatinib and carvedilol) in the cells and this causes a decrease
353 in the virus binding with OATP1A2. Another possibility is that the substrates and inhibitors
354 can directly bind to OATP1A2 on the cell surface, which results in a decrease of CaHEV
355 attachment and infection; specific mechanisms need to be further explored to determine this.
356 Notably, these results implied that the substrates or inhibitors of OATP1A2 can be used as
357 therapeutic drugs to prevent or cure HEV infection.

358 In conclusion, this is the first study to document that the host protein OATP1A2 can
359 directly interact with the avian HEV capsid protein. Also, the expression levels of OATP1A2
360 in host cells can influence avian HEV attachment and infection of the cells *in vitro*.
361 Additionally, the distribution of OATP1A2 in chicken tissues positively corresponds with
362 tissues targeted by avian HEV *in vivo*. In addition, the substrates and inhibitors of OATP1A2
363 as well as blocking OATP1A2 with ap237 and anti-1A2^{ecto} sera can significantly reduce
364 avian HEV attachment and infection. These findings offer new clues to understand the
365 mechanism of avian HEV infection and may provide a theoretical basis and guidance for the
366 prevention of HEV infection, its treatment, and vaccine development.

367

MATERIALS AND METHODS

Virus and cells. An avian HEV infectious stock was produced by intravenously inoculating four 8-week-old specific pathogen-free (SPF) chickens with 200 µL of a clinical bile sample containing avian HEV (CaHEV, GenBank accession no. GU954430) from a 35-week-old broiler breeder chicken in China (14). At 21 days post-inoculation, virus-positive fecal samples were collected and suspended in PBS buffer (10 mM, pH 7.2). After centrifugation at 6200 × *g* at 4°C for 10 minutes, the supernatant was incubated with 8% PEG 8000 (Sigma Chemical Co., St. Louis, MO, USA) at 4°C overnight. Following this, the mixture was centrifuged at 13,000 × *g* for 1 hour again, and the pellet was suspended with PBS buffer and filtered with a 0.22 µm filter. This virus stock was stored at -80°C.

Human embryo kidney HEK 293T cells, DF-1 cells and the LMH cell line were purchased from the American Type Culture Collection (ATCC) and grown in Dulbecco's modified Eagle's medium (DMEM; Gibco, Carlasbad, CA, USA) supplemented with 10% fetal bovine serum (FBS, Gibco, Carlasbad, CA, USA), 100 U/mL penicillin (Life Technologies Corp., Grand Island, NY, USA), and 100 µg/mL streptomycin (Life Technologies Corp., Grand Island, NY, USA). All of the cell lines were cultured at 37°C in a humidified atmosphere with 5% CO_2.

Primary cultured chicken embryo hepatocytes (CEH) were isolated from a 19-day-old SPF chicken embryo purchased from Beijing Merial Vital Laboratory Animal Technology Company. Liver tissue was immersed in D-Hank's buffer, minced and washed three times to remove the red blood cells, and then trypsinized for 10-15 minutes. After centrifugation, the cell pellet containing chicken hepatocytes was resuspended in growth medium of M199 medium (Gibco, Carlasbad, CA, USA) supplemented with 10% FBS, 5 µg/mL transferrin (ThermoFisher Scientific, CA, USA), 10 ng/mL EGF (ThermoFisher Scientific, CA, USA),

40 ng/mL dexamethasone (Acros Organic, Belgium, USA), 3 μg/mL insulin (Gibco, Carlasbad, CA, USA), 2 mM L-glutamine (Gibco, Carlasbad, CA, USA), 100 U/mL penicillin and 100 μg/mL streptomycin. The cells were counted and plated on collagen-coated cell culture dishes or plates. Cells were maintained in 5% CO_2 humidified incubator at 37°C. After plated for 12 hours, the culture medium was changed and then the regular medium was changed every 2-3 days.

For GST pull-down assays, the CEH cells were pelleted through centrifugation at 600 × *g* at 4°C. Then, the cell pellet was resuspended with PBS, and then was counted and packed at 1×10^7 cells per tube. After centrifugation, cell pellets were resuspended and lysed with NP-40 buffer (Beyotime, Shanghai, China) on ice for 30 min, and then the supernatant was collected by centrifugation and used to perform GST pull-down assays.

Plasmid construction. To produce the bait protein for the GST pull-down assay, a recombinant plasmid containing the truncated ORF2 gene encoding ap237 was constructed with the pGEX-6P-1 vector (GE Healthcare, New Jersey, USA) with an N-terminal GST tag as the backbone. Briefly, the truncated ORF2 gene encoding ap237 was amplified with the primer pairs GST-ap237-F/R and cloned into the vector. The positive recombinant plasmid was designated pGEX-6P-1-ap237. In addition, in order to express another form of ap237 without the tag protein, the truncated gene was also amplified with primer pairs Ap237-F/R and cloned into the pET-21b (Novagen, Darmstadt, Germany) vector for bacterial expression. The recombinant plasmid was named pET-21b-ap237. To generate the eukaryotic expression vector for the co-immunoprecipitation (Co-IP) assay, the truncated ORF2 gene was amplified with the primer pair HA-ap237-F/R and cloned into the pCAGEN vector (47) with an N-terminal HA tag. The positive plasmid was named pCAGEN-HA-ap237.

In order to interact with the host protein OATP1A2, two different eukaryotic expression vectors were constructed. Firstly, based on the coding sequence of OATP1A2 (GenBank

417 accession no. XM_416421.6), the primer pair OATP1A2-F/R was designed and used to
418 amplify the complete coding sequence from the chicken liver cDNA library. Then, for the Co-
419 IP assay, the gene was cloned into the p×3Flag-CMV-14 expression vector (Sigma-Aldrich,
420 St. Louis, MO, USA) with a C-terminal 3×Flag tags, and the recombinant plasmid was
421 named pCMV-1A2-3Flag. To construct the LMH cell lines with stable expression of
422 OATP1A2, the gene was inserted into the pTrip-puro lentivirus vector. To facilitate the
423 screening of positive cells, OATP1A2 was fused with a GFP coding sequence with a linker
424 sequence (5'-TCCGGCCGGACTCAGATCTCGAGCTCAAGCTTCGAATTCAAA-3'),
425 including 14 amino acids (48), using primers pairs of 1A2-F/1A2-linker-R and linker-GFP-
426 F/GFP-R by overlapping PCR. The PCR product was inserted into the vector and the positive
427 plasmid was named pTrip-1A2-GFP-puro or pTrip-GFP-puro. For the constructing of pTrip-
428 GFP-puro, the GFP sequence was amplified with the primer pairs GFP-F/R and cloned into
429 the pTrip-puro vector. In addition, in order to produce antiserum against OATP1A2 and
430 evaluate the direct interaction between ap237 with OATP1A2, the transmembrane helices of
431 OATP1A2 were predicted by the TMHMM server (v. 2.0) (49). The gene sequences encoding
432 extracellular domains were connected and synthesized by Genewiz, Inc. (Suzhou, China), and
433 ligated into the pGEX-6P-1 vector for expression. The transmembrane region of OATP1A2
434 was designated as $1A2^{ecto}$, and the positive recombinant plasmid was named pGEX-6P-1-
435 $1A2^{ecto}$.

436 All primers used in the study are listed in Table 2.

437 **Protein expression in bacteria.** To express GST-ap237 and GST-$1A2^{ecto}$ in a bacterial
438 system, recombinant plasmids pGEX-6P-1-ap237 and pGEX-6P-1-$1A2^{ecto}$ were separately
439 transformed into *Escherichia coli* (*E. coli*) Transetta (DE3) (TransGen Biotech, Beijing,
440 China). Then, the two proteins were induced by 0.2 mM isopropyl-β-D-thiogalactoside
441 (IPTG) for 20 hours at 16°C. After that, the bacteria were sonicated and clarified. The two

442 soluble proteins were filtered with a 0.22 μm filter and purified with the Glutathione
443 Sepharose 4 Fast Flow system (GE Healthcare, Uppsala, Sweden). The expression and
444 purification of the proteins were analyzed by SDS-PAGE and Western blot using anti-GST
445 antibodies and 3E8 monoclonal antibody (mAb) (19, 22) against the avian HEV ORF2
446 protein as the primary antibody for ap237 detection.

447 The procedure for inducing the expression of ap237 without any tags was based on the
448 modified methods described by Chen et al. (50). Briefly, the expression of ap237 was induced
449 by adding 1.0 mM IPTG for 6-8 hours at 37°C. Bacterial cells were harvested and lysed by
450 sonication. The cell pellets were dissolved in 8M urea, filtered with a 0.22 μm filter, refolded
451 with gradient buffer (6M urea, 4M urea, 2M urea in PBS), and purified using a Superdex 200
452 Increase 10/300 GL Column (GE Healthcare, New Jersey, USA) connected to an ÄKTA
453 purifier (GE Healthcare, New Jersey, USA). Then, the expression and purification of ap237
454 was analyzed by SDS-PAGE and Western blot using 3E8 mAb as the primary antibody.

455 The control proteins used in this study were truncated capsid proteins (aa 368-606),
456 which included sar239, ker239, r239, and sp239; these were from genotype 1 human HEV
457 (Sar-55, AF444002), genotype 3 human HEV (Kernow-C1, JQ679013), genotype 3 rabbit
458 HEV (CHN-SX-rHEV, KX227751), and genotype 4 swine HEV (CHN-SD-sHEV,
459 KE176351), respectively, and were all expressed and purified as previously described by
460 Chen et al. (50). Another negative control protein, the porcine reproductive and respiratory
461 syndrome virus (PRRSV) N protein, was also expressed and purified according to the same
462 above procedures.

463 **GST pull-down assay and mass spectrometry assay.** For the GST pull-down assays,
464 GST or GST-ap237 proteins were separately conjugated to Glutathione Sepharose beads and
465 then blocked with 5% bovine serum albumin for 1 hour. After washing three times with PBS,
466 the two beads were separately incubated for 8-12 hours at 4°C with the chicken liver cell

lysis treated with NP-40 buffer. After washing three times again, the two beads were transferred to a new tube. Finally, the binding proteins were eluted by elution buffer (50 mM Tris-HCl containing 10 mM reduced glutathione, pH 8.0) and analyzed by SDS-PAGE with silver staining. The specific bands for GST-ap237 were cut and mixed together, and subsequently analyzed by mass spectrometry (MS). MS was performed using the Q Exactive HF Orbitrap LC-MS/MS System at the Research Center for Proteome Analysis, Shanghai Institutes for Biological Sciences, Chinese Academy of Sciences, China. After acquiring the raw data, Mascot 2.2 (Matrix Science, MA, USA) (51) was used to retrieve the *Gallus gallus* UniProt database (52, 53) and obtained the score, coverage, peptides, and peptide spectrum match (PSM) values of all the proteins.

In addition, the GST pull-down assay was also performed to confirm direct interaction between OATP1A2 and ap237. The GST or GST-1A2^{ecto} proteins were separately conjugated to Glutathione Sepharose beads and then incubated for 8-12 hours at 4°C with ap237. After washing, the eluted proteins were analyzed by Western blot using 3E8 mAb and anti-GST antibodies as the primary antibodies. The sp239 protein was used as the negative control.

Production of antisera against GST-1A2^{ecto}. Five 7-week-old BALB/c mice were immunized intraperitoneally with purified GST-1A2^{ecto} protein at a dose of 100 μg per mouse, which was emulsified with Freund's complete adjuvant (Sigma-Aldrich, St. Louis, MO, USA). The mice were boosted in 14-day intervals with the same dose of antigen in Freund's incomplete adjuvant. To obtain negative serum eliminating the interference of the GST tag antibody, another five mice were immunized with only the GST tag protein according to the same method. Seven days after the second boost, blood was collected at the tail vein. Following this, the titers of anti-GST-1A2^{ecto} antibodies in the sera were determined with indirect ELISA.

491 **Co-immunoprecipitation and confocal immunofluorescence assay.** To confirm the
492 interaction of ap237 and OATP1A2, a cell-based Co-IP assay was performed as follows.
493 Briefly, the pCAGEN-HA-ap237 and pCMV-1A2-3Flag plasmids were co-transfected into
494 HEK 293T cells for 48 hours. Next, the cells were lysed with NP-40 lysis buffer containing 1
495 mM phenylmethylsulfonyl fluoride (Sigma Chemical Co., St. Louis, MO, USA) on ice for 30
496 minutes and clarified by centrifugation at 12,000 × *g* for 15 min at 4°C. After centrifugation,
497 the clarified supernatant was subjected to immunoprecipitation using Dynabeads® Protein G
498 (ThermoFisher Scientific, CA, USA) bound to the anti-HA mAb (ProteinTech, Wuhan, China)
499 or the anti-Flag mAb (Sigma-Aldrich, St. Louis, MO). The immunoprecipitates were then
500 resolved by 10% SDS-PAGE. The bound proteins were detected by Western blot using the
501 anti-Flag and the anti-HA mAbs. The recombinant plasmid pCAGEN-HA-ORF3 and two
502 empty vectors, including pCAGEN-HA and pCMV-3Flag were used as controls.

503 In addition, the co-transfected HEK 293T cells were also used to perform a confocal
504 immunofluorescence assay for analyzing the co-location of ap237 and OATP1A2 in the cells.
505 After co-transfection for 48 hours, the washed cells were fixed with 4% paraformaldehyde
506 (Solarbio Life Science, Beijing, China) for 15 min at 37°C and permeabilized with 0.25%
507 Triton X-100 for 15 min at 37°C. After washing three times with PBS buffer, the cells were
508 incubated with 1% bovine serum albumin in PBS for 1 hour at 37°C for blocking. Next, they
509 were incubated with the rabbit anti-FLAG polyclonal antibodies (ProteinTech, Chicago, USA)
510 and the anti-HA mAb for 1 hour at 37°C. After washing again, they were incubated for 1 hour
511 with Alexa Fluor® 488-conjugated AffiniPure Goat Anti-Mouse IgG (H+L) and Cy3-
512 conjugated Goat Anti-Rabbit IgG (H+L) (Jackson ImmunoResearch, West Grove, PA, USA).
513 Finally, the cells were fixed with Fluoroshield™ with DAPI (Sigma-Aldrich, St. Louis, MO,
514 USA) and observed with a Leica SP8 confocal system (Leica, Wetzlar, Germany). The co-
515 localization of ap237 and OATP1A2 was evaluated by the determination of Manders' overlap

516 coefficient using Image-plus pro software. Manders' overlap coefficient indicates an actual
517 overlap of the fluorescence signals (54). This value ranging from 0 to 1.0 implies 0% to
518 100% of both selected channels co-localization.

519 **Indirect ELISA.** To test the direct interaction of the avian HEV capsid protein and
520 chicken OATP1A2, an indirect ELISA was performed as follows. The 96-well ELISA plates
521 were coated with different dosages of ap237 (8 μg/well, 4 μg/well, 2 μg/well, and 1 μg/well)
522 dissolved in PBS buffer (pH 7.2) and incubated for 12 hours at 4°C. After washing, the plates
523 were incubated with blocking buffer consisting of 2.5% dry milk in 0.05% Tween 20 in PBS
524 (PBST) for 1 hour at 37°C. Plates were then incubated with differing concentrations of GST-
525 1A2^{ecto} (200 μg/mL, 20 μg/mL, 2 μg/mL, and 0.2 μg/mL) and GST (100 μg/mL, 10 μg/mL, 1
526 μg/mL, and 0.1 μg/mL) with 100 μL/well for 1 hour at 37°C. After washing, the plates were
527 treated with blocking buffer and incubated for 1 hour at 37°C. Following this, the anti-GST
528 antibodies at a dilution of 1:1000 were added to the wells. After an incubation of 1 hour at
529 37°C, HRP-conjugated goat anti-mouse IgG antibody (Jackson ImmunoResearch, West
530 Grove, PA, USA) was added to the wells at a dilution of 1:5000. The colorimetric reaction
531 was triggered by the addition of tetramethylbenzidine (Sigma Chemical Co., St. Louis, MO,
532 USA) for 15 min and stopped by the addition of 3M H_2SO_4. The OD_{450nm} value was read
533 using an automated ELISA plate reader (Bio-Rad, CA, USA). In order to analyze the
534 interaction of chicken OATP1A2 with capsid proteins of HEVs of the other species, sar239,
535 ker239, r239, and sp239 were also coated in 96-well ELISA plate wells and then incubated
536 with GST-1A2^{ecto} (20 μg/mL) and GST (10 μg/mL). In addition, the PRRSV N protein was
537 also coated in the wells as the negative control protein.

538 To identify the interaction of OATP1A2 with the soluble ORF2 proteins in avian HEV
539 infected chicken serum, 300 μL positive sera were added to the ELISA plate coated with
540 mAb 3E8 (800ng/well). After incubation and washing, GST-1A2^{ecto} and the control of GST

were added and followed by washing and the incubation with rabbit anti-GST antibody. HRP-goat anti-rabbit IgG antibody (Jackson ImmunoResearch, West Grove, PA, USA) was used as the secondary antibody.

Quantitative real time PCR (qPCR) for quantifying OATP1A2 RNA. To quantify the expression of OATP1A2 RNA in chicken tissues and different cell lines, the total RNA of each tissue or cell line was extracted using the High Pure RNA Isolation Kit (Roche, Manheim, Germany). The mRNA levels were quantified using the StepOnePlus™ Real-Time PCR System (Applied Biosystems, Foster City, CA, USA) and FastStart Universal SYBR Green Master Mix (ROX) (Roche, Manheim, Germany). Specific primers used were designed as previously reported (55) and are shown in Table 2. An endogenous gene GAPDH was used as the reference gene with the primers listed in Table 2. The mRNA levels were calculated using the 2-△△Ct method with GAPDH as an endogenous reference.

Establishment of cell lines with stable expression of OATP1A2. The lentivirus gene transfer system was applied to generate cell lines constitutively expressing the recombinant OATP1A2-GFP protein. The cell line with stable expression of the GFP protein was also established as the control. Briefly, to produce replication-defective lentivirus stocks, the HEK 293T cells were co-transfected with 2 μg pTrip-1A2-GFP-puro or 2 μg pTrip-GFP-puro with packing plasmids pFIV-34N (System Biosciences, CA, USA) (3 μg) and pVSV-G (3 μg) (System Biosciences, CA, USA). Three days after transfection, cell supernatants containing recombinant lentivirus were harvested and used to infect the target LMH cells. At 48 hours post-infection, LMH cells with a stable expression of OATP1A2-GFP and those expressing only GFP were selected with 4 μg/mL puromycin. OATP1A2 expression was detected by indirect fluorescence assay using mouse anti-GST-1A2^{ecto} sera and Tetramethylrhodamine (TIRTC) conjugated goat anti-mouse IgG (Jackson ImmunoResearch, West Grove, PA, USA). The puromycin-resistant and the green cell clones were examined by qPCR to determine the

566 presence of OATP1A2 and GFP. Then, the established cell lines were separately named
567 LMH$^{1A2\text{-}GFP}$ and LMH^{GFP}. In addition, to determine the expression location of OATP1A2-
568 GFP in the LMH$^{1A2\text{-}GFP}$ cell line, the membrane proteins were extracted for Western blot to
569 detect the target OATP1A2 using the Mem-PER™ Plus Membrane Protein Extraction Kit
570 (Thermo scientific, Waltham, MA, USA) according to the manufacturer's instructions. In
571 addition, the expression and location of OATP1A2 in CEH were also identified with mouse
572 anti-GST-1A2^{ecto} sera using confocal immunofluorescence and Western blot.

573 **RNA interference to knockdown the expression of OATP1A2.** To knockdown the
574 expression of OATP1A2 in the cell line LMH$^{1A2\text{-}GFP}$, three siRNAs targeting OATP1A2 and a
575 negative control were designed and synthesized from RiboBio Company (RiboBio,
576 Guangzhou, China). The siRNA target sequences were CACAGATAGAGAAGCAATT
577 (si1A2-1), CCAAACAGAGCATGTATGA (si1A2-2), and TGAAAGGAATGTCTCATTA
578 (si1A2-3). The LMH$^{1A2\text{-}GFP}$ cells were transfected with the siRNAs using Lipofectamine®
579 RNAiMAX (Invitrogen, CA, USA) reagent. After transfection, the qPCR and Western blot
580 assays were used to analyze the expression of OATP1A2 in the transfected cells.

581 **Ap237 attachment to different cell lines.** In a previous study, it was documented that
582 ap237 can imitate natural avian HEV particles and attach to LMH cells (30). In this study, the
583 variations of ap237 attachment to differently-treated LMH cell lines expressing different
584 levels of OATP1A2 were firstly analyzed. The different cell lines (LMH$^{1A2\text{-}GFP}$, LMH,
585 LMH^{GFP}, and LMH$^{1A2\text{-}GFP}$ transfected siRNA) were seeded on six-well plates with the
586 concentration of 1.6×10^{6}/well. After culturing for 24 hours (with a confluence of 70%-90%),
587 the cells were washed gently with cold PBS and incubated with 500 nM ap237 (or 5 μM for
588 the flow cytometry assay) diluted with DMEM for 1 hour at 4°C. Finally, the amount of
589 ap237 attached to the cells was determined by Western blot and flow cytometry assays. The
590 mAb 3E8 was used as primary antibody to target ap237 in the assays.

591 **TaqMan real-time RT-PCR for quantifying avian HEV RNA.** For determining the
592 amount of CaHEV**,** a TaqMan real-time RT-PCR was developed and performed in a 20-
593 reaction mixture on the Applied Biosystem StepOnePlus™ Real-Time PCR system (Applied
594 Biosystems, Foster City, CA, USA) using the QuantiTect Probe RT-PCR kit (Qiagen, Hilden,
595 Germany). The primers and probe targeting ORF3 were designed as in a previous report (56)
596 and is shown in Table 2. The cDNA from RNA was synthesized via reverse transcription for
597 30 min at 50°C followed by the PCR initial activation step for 15 min at 95°C. Next,
598 targeting ORF3 was amplified for 45 cycles at 94°C for 15 s and 60°C for 60 s. In addition,
599 to generate the internal control RNA, a 174 bp RT-PCR product was amplified using the
600 primers of Taqman-T7f and Taqman-R (Table 2), and then cloned into the pMD19-T vector
601 (TaKaRa Biotech Corporation, Dalian, China). The vectors were linearized using the Pst I
602 restriction enzyme (TaKaRa Biotech Corporation, Dalian, China) and purified by the Wizard®
603 DNA Clean-Up System (Promega, Madison, WI, USA), according to the manufacturer's
604 protocol. Then, the purified plasmid DNA was transcribed *in vitro* using a RiboMAX™
605 Large Scale RNA Production System-T7 (Promega, Madison, WI, USA). The concentration
606 of RNA was determined at least four times by a spectrophotometer (BioTek Instruments Inc.,
607 Belgium, WI, USA), and the number of copies per µl were calculated using the mean values
608 and the following formula: $[(g/\mu l\ RNA)/(length \times 340)] \times 6.022 \times 10^{23}$, where the length is
609 the number of nucleotides.

610 **Avian HEV attachment and infection of differently-treated cell lines.** Although there
611 are no highly effective cell culture systems for avian HEV infection, the virus can attach and
612 infect LMH cells at low levels (32, 57). The relationship between avian HEV infection and
613 OATP1A2 expression levels was also evaluated in the differently-treated LMH cell lines;
614 however, the amount of avian HEV was only detected by TaqMan real-time RT-PCR. For the
615 attachment assay, LMH, $LMH^{1A2\text{-}GFP}$, LMH^{GFP}, and $LMH^{1A2\text{-}GFP}$ transfected with siRNA cells

were seeded on 12-well plates with a concentration of 8×10^5/well and cultured at 37°C and 5% CO_2. When the cell confluence was approximately 80%, the cells were inoculated with CaHEV virus (1×10^6 HEV RNA copies) diluted with DMEM and 2% (w/v) FBS. After 2 hours of incubation at 4°C, the cells were washed three times with cold PBS and collected using the RNAiso Plus reagent (TaKaRa Biotech Corporation, Dalian, China) to extract the total RNA. For the infection assay, the procedures were similar to the attachment assay, except after the cells were inoculated with CaHEV virus diluted with DMEM, the cells were cultured at 37°C and half of the maintenance medium was changed every 2 days. To determine the viral replication in the cells, the infected cells were collected at various days post-infection. Following this, the total RNA was extracted for quantifying the viral RNA by TaqMan real-time RT-PCR. The negative-strand viral ORF3 RNA was also detected using negative-strand-specific RT-PCR developed by Billiam et al (58) with the primer pairs of EF1/ER1 and EF2/ER2 (Table 2) for further identifying the viral replication in the cells.

Next, the variations of avian HEV attachment and infection of $LMH^{1A2\text{-}GFP}$ cells were evaluated when the cells were treated with different substrates and the inhibitor of OATP1A2. The inhibitor, carvedilol (Adamas, Shanghai, China), and the substrates, including chenodeoxycholic acid (Acros Organic, Belgium, USA), sodium cholate and imatinib (Sigma Chemical Co., St. Louis, MO, USA), were pre-incubated with $LMH^{1A2\text{-}GFP}$ cells in at 37°C and 5% CO_2 for 24 hours. Subsequently, the treated $LMH^{1A2\text{-}GFP}$ cells were inoculated with CaHEV and the total RNA was extracted in the same manner as above.

In addition, avian HEV attachment and infection of $LMH^{1A2\text{-}GFP}$ cells was also analyzed when the OATP1A2 in the cells was blocked with ap237 and anti-GST-$1A2^{ecto}$ mouse sera. The $LMH^{1A2\text{-}GFP}$ cells were firstly incubated with ap237 and anti-GST-$1A2^{ecto}$ mouse sera at 37°C and 5% CO_2 for 24 hours and then were inoculated with the CaHEV virus as described above. The sp239 and negative mouse sera were used as the negative control protein and

641 negative control sera.

642 To further confirm that the OATP1A2 is involved in avian HEV infection in the host
643 cells, the CEH cells were treated with imatinib, ap237, and anti- GST-1A2^{ecto} mouse sera and
644 then inoculated with CaHEV. The total RNA was extracted and used as the template to detect
645 viral RNA copies.

646 **Avian HEV infection of chickens.** Six 8-week-old SPF chickens were purchased from
647 Beijing Merial Vital Laboratory Animal Technology Company. All chickens were negative
648 for avian HEV antibodies and RNA. The chickens were housed together and intravenously
649 inoculated with the same dose of viral stock (1×10^6 CaHEV RNA copies). At 3 weeks post-
650 inoculation, the different tissues, including tongue, esophagus, crop, glandular stomach,
651 muscle stomach, duodenum, jejunum, ileum,cecum, rectum, liver, gallbladder, bile duct,
652 pancreas, spleen, heart, lung, kidney, testis (or ovary), brain, spinal cord, nerve, thymus, and
653 muscle were collected to detect CaHEV and OATP1A2. In addition, fecal samples were
654 collected to detect CaHEV RNA in order to confirm successful infection.

655 **Immunohistochemistry assay.** Healthy paraffin-embedded sections from CaHEV-
656 infected chicken tissues (3 μm) were prepared by Yangling Yike Company. Sections were
657 deparaffinized by heating in an oven at 60°C, rehydrated, and then endogenous peroxidase
658 activity was eliminated using 3% H_2O_2 in deionized water. Sections were immersed in 10
659 mM sodium citrate (pH 6.0) to heat-induce antigen retrieval. Immunochemical staining was
660 performed by following the instructions of Ready-to-use SAB-POD (Mouse IgG) Kit
661 (BOSTER, Wuhan, China). Briefly, after blocking 30 minutes at 37°C with 5% BSA, mouse
662 anti-GST-1A2^{ecto} serum diluted in blocking buffer (1:100) was added and incubated overnight
663 at 4°C; PBS and mouse anti-GST serum were used as negative controls. Subsequently,
664 sections were washed three times and incubated with biotinylated goat anti-mouse IgG for 30

minutes at 37°C, followed by rinsing and incubation with SABCs (streptavidin–biotin complexes) at 37°C for 30 minutes. After washing, the immune reaction was visualized using DAB substrate and nuclei were counterstained with hematoxylin. Finally, the dehydration and transparency of sections were performed and sections were mounted to observe under a microscope.

Computer analysis. To predict the spatial locations of ap237, the 3D model of the avian HEV capsid protein was built by SWISS-MODEL (59), using advanced remote homology detection methods based on the established crystal structure of the HEV capsid protein, deposited as entry 2ZTN (23) within the Research Collaboratory for Structural Bioinformatics Protein Data Bank. Following this, the areas of interest were visually highlighted with different colors using CHIMERA software (60). In addition to this, OATP1A2 structure was predicted using the Phyre2 web portal (61), based on the d1pw4a template.

Statistical analyses. The data from qPCR and TaqMan real-time RT-PCR assays and cell viability assays was evaluated using GraphPad Prism, version 6 (GraphPad Software, Inc., La Jolla, CA, USA). Statistical differences among the groups were calculated using one-way ANOVA. P values are indicated in the figures.

Ethics statement. All animal experiments were performed according to the Guidance for Experimental Animal Welfare and Ethical Treatment by the Ministry of Science and Technology of China (www.most.gov.cn/fggw/zfwj/zfwj2006/zf06yw/zf06qt/200612/t20061226_39235.htm). Experimental procedures and animal use and care protocols were carried out in accordance with the guidelines of the Northwest A&F University Institutional Animal Use and Care

688 Committee and were approved by the Committee on Ethical Use of Animals of Northwest
689 A&F University.
690

691 **ACKNOWLEDGEMENTS**

692 H.L. performed the research, analyzed data, and drafted the paper. M.F., B.L., P.J.,
693 and Y.C. contributed to the construction of cell lines. B.Z., Y.S., and B.H. contributed to the
694 immunohistochemistry assay. Y.N. and Z.S. contributed to the confocal immunofluorescence
695 assay. J.P.S and J.A.H. contributed to the mass spectrometry assay data analysis. Q.Z. and E.-
696 M.Z. conceived the study, carried out additional analyses, and finalized the paper. All authors
697 contributed to revising the manuscript.

698 This study was supported by grants from the National Natural Science Foundation of
699 China to E.-M.Z. (31720103919) and Q.Z. (31672583). Q.Z. is a Tang Scholar of Northwest
700 A&F University recipient.

701

REFERENCES

1. **Smith DB, Simmonds P, International Committee on Taxonomy of Viruses Hepeviridae Study G, Jameel S, Emerson SU, Harrison TJ, Meng XJ, Okamoto H, Van der Poel WH, and Purdy MA.** 2014. Consensus proposals for classification of the family Hepeviridae. J Gen Virol **95:**2223-2232.
2. **Johne R, Dremsek P, Reetz J, Heckel G, Hess M, and Ulrich RG.** 2014. Hepeviridae: an expanding family of vertebrate viruses. Infect Genet Evol **27:**212-229.
3. **Haqshenas G, Shivaprasad HL, Woolcock PR, Read DH, and Meng XJ.** 2001. Genetic identification and characterization of a novel virus related to human hepatitis E virus from chickens with hepatitis-splenomegaly syndrome in the United States. Journal of General Virology **82:**2449-2462.
4. **Clarke JK, Allan GM, Bryson DG, Williams W, Todd D, Mackie DP, and McFerran JB.** 1990. Big liver and spleen disease of broiler breeders. Avian Pathol **19:**41-50.
5. **Zhao Q, Liu B, Sun Y, Du T, Chen Y, Wang X, Li H, Nan Y, Zhang G, and Zhou EM.** 2017. Decreased egg production in laying hens associated with infection with genotype 3 avian hepatitis E virus strain from China. Vet Microbiol **203:**174-180.
6. **Handlinger JH, and Williams W.** 1988. An egg drop associated with splenomegaly in broiler breeders. Avian Dis **32:**773-778.
7. **Gerber PF, Trampel DW, Willinghan EM, Billam P, Meng XJ, and Opriessnig T.** 2015. Subclinical avian hepatitis E virus infection in layer flocks in the United States. Veterinary Journal **206:**304-311.
8. **Troxler S, Pac K, Prokofieva I, Liebhart D, Chodakowska B, Furmanek D, and Hess M.** 2014. Subclinical circulation of avian hepatitis E virus within a multiple-age rearing and broiler breeder farm indicates persistence and vertical transmission of the virus. Avian Pathology **43:**310-318.
9. **Billam P, Huang FF, Sun ZF, Pierson FW, Duncan RB, Elvinger F, Guenette DK, Toth TE, and Meng XJ.** 2005. Systematic pathogenesis and replication of avian hepatitis E virus in specific-pathogen-free adult chickens. J Virol **79:**3429-3437.
10. **Banyai K, Toth AG, Ivanics E, Glavits R, Szentpali-Gavaller K, and Dan A.** 2012. Putative novel genotype of avian hepatitis E virus, Hungary, 2010. Emerg Infect Dis **18:**1365-1368.
11. **Bilic I, Jaskulska B, Basic A, Morrow CJ, and Hess M.** 2009. Sequence analysis and comparison of avian hepatitis E viruses from Australia and Europe indicate the existence of different genotypes. J Gen Virol **90:**863-873.
12. **Hsu IW, and Tsai HJ.** 2014. Avian hepatitis E virus in chickens, Taiwan, 2013. Emerg Infect Dis **20:**149-151.
13. **Kwon HM, Sung HW, and Meng XJ.** 2012. Serological prevalence, genetic identification, and characterization of the first strains of avian hepatitis E virus from chickens in Korea. Virus Genes **45:**237-245.
14. **Zhao Q, Zhou EM, Dong SW, Qiu HK, Zhang L, Hu SB, Zhao FF, Jiang SJ, and Sun YN.** 2010. Analysis of avian hepatitis E virus from chickens, China. Emerg Infect Dis **16:**1469-1472.
15. **Meng XJ.** 2010. Hepatitis E virus: animal reservoirs and zoonotic risk. Vet Microbiol **140:**256-265.
16. **Huang FF, Sun ZF, Emerson SU, Purcell RH, Shivaprasad HL, Pierson FW, Toth TE, and Meng XJ.** 2004. Determination and analysis of the complete genomic sequence of avian hepatitis E virus (avian HEV) and attempts to infect rhesus monkeys with avian HEV. J Gen Virol **85:**1609-1618.
17. **Li TC, Suzaki Y, Ami Y, Dhole TN, Miyamura T, and Takeda N.** 2004. Protection

of cynomolgus monkeys against HEV infection by oral administration of recombinant hepatitis E virus-like particles. Vaccine **22:**370-377.

18. **Zhou EM, Guo H, Huang FF, Sun ZF, and Meng XJ.** 2008. Identification of two neutralization epitopes on the capsid protein of avian hepatitis E virus. J Gen Virol **89:**500-508.
19. **Dong S, Zhao Q, Lu M, Sun P, Qiu H, Zhang L, Lv J, and Zhou EM.** 2011. Analysis of epitopes in the capsid protein of avian hepatitis E virus by using monoclonal antibodies. J Virol Methods **171:**374-380.
20. **Zhao Q, Syed SF, and Zhou EM.** 2015. Antigenic properties of avian hepatitis E virus capsid protein. Vet Microbiol **180:**10-14.
21. **Surjit M, Jameel S, and Lal SK.** 2007. Cytoplasmic localization of the ORF2 protein of hepatitis E virus is dependent on its ability to undergo retrotranslocation from the endoplasmic reticulum. Journal of Virology **81:**3339-3345.
22. **Wang L, Sun Y, Du T, Wang C, Xiao S, Mu Y, Zhang G, Liu L, Widen F, Hsu WH, Zhao Q, and Zhou EM.** 2014. Identification of an antigenic domain in the N-terminal region of avian hepatitis E virus (HEV) capsid protein that is not common to swine and human HEVs. J Gen Virol **95:**2710-2715.
23. **Yamashita T, Mori Y, Miyazaki N, Cheng RH, Yoshimura M, Unno H, Shima R, Moriishi K, Tsukihara T, Li TC, Takeda N, Miyamura T, and Matsuura Y.** 2009. Biological and immunological characteristics of hepatitis E virus-like particles based on the crystal structure. Proceedings of the National Academy of Sciences of the United States of America **106:**12986-12991.
24. **He S, Miao J, Zheng Z, Wu T, Xie M, Tang M, Zhang J, Ng MH, and Xia N.** 2008. Putative receptor-binding sites of hepatitis E virus. J Gen Virol **89:**245-249.
25. **Zheng ZZ, Miao J, Zhao M, Tang M, Yeo AET, Yu H, Zhang J, and Xia NS.** 2010. Role of heat-shock protein 90 in hepatitis E virus capsid trafficking. Journal of General Virology **91:**1728-1736.
26. **Shen Q, Zhang W, Kang Y, Chen Y, Cui L, Yang Z, and Hua X.** 2011. HEV-Capsid Protein Interacts With Cytochrome P4502C8 and Retinol-Binding Protein 4. Hepat Mon **11:**913-917.
27. **Kalia M, Chandra V, Rahman SA, Sehgal D, and Jameel S.** 2009. Heparan sulfate proteoglycans are required for cellular binding of the hepatitis E virus ORF2 capsid protein and for viral infection. J Virol **83:**12714-12724.
28. **Zhang L, Tian YB, Wen ZH, Zhang F, Qi Y, Huang WJ, Zhang HQ, and Wang YC.** 2016. Asialoglycoprotein receptor facilitates infection of PLC/PRF/5 cells by HEV through interaction with ORF2. Journal of Medical Virology **88:**2186-2195.
29. **Tian Y, Huang W, Yang J, Wen Z, Geng Y, Zhao C, Zhang H, and Wang Y.** 2017. Systematic identification of hepatitis E virus ORF2 interactome reveals that TMEM134 engages in ORF2-mediated NF-kappaB pathway. Virus Res **228:**102-108.
30. **Zhang XQ, Bilic I, Marek A, Glosmann M, and Hess M.** 2016. C-Terminal Amino Acids 471-507 of Avian Hepatitis E Virus Capsid Protein Are Crucial for Binding to Avian and Human Cells. Plos One **11**.
31. **Kawaguchi T, Nomura K, Hirayama Y, and Kitagawa T.** 1987. Establishment and characterization of a chicken hepatocellular carcinoma cell line, LMH. Cancer Res **47:**4460-4464.
32. **Huang FF, Pierson FW, Toth TE, and Meng XJ.** 2005. Construction and characterization of infectious cDNA clones of a chicken strain of hepatitis E virus (HEV), avian HEV. J Gen Virol **86:**2585-2593.
33. **Li SW, Zhang J, Li YA, Ou SH, Huang GY, Huang GY, He ZQ, Ge SX, Xian YL, Pang SQ, Ng MH, and Xia NS.** 2005. A bacterially expressed particulate hepatitis E

vaccine: antigenicity, immunogenicity and protectivity on primates. Vaccine **23:**2893-2901.

34. **Lee W, Glaeser H, Smith LH, Roberts RL, Moeckel GW, Gervasini G, Leake BF, and Kim RB.** 2005. Polymorphisms in human organic anion-transporting polypeptide 1A2 (OATP1A2): implications for altered drug disposition and central nervous system drug entry. J Biol Chem **280:**9610-9617.
35. **Kullakublick GA, Hagenbuch B, Stieger B, Schteingart CD, Hofmann AF, Wolkoff AW, and Meier PJ.** 1995. Molecular and Functional-Characterization of an Organic Anion Transporting Polypeptide Cloned from Human Liver. Gastroenterology **109:**1274-1282.
36. **Gaudet P, Livstone MS, Lewis SE, and Thomas PD.** 2011. Phylogenetic-based propagation of functional annotations within the Gene Ontology consortium. Briefings in Bioinformatics **12:**449-462.
37. **Ritchie SJ, and Riddell C.** 1991. British Columbia. "Hepatitis-splenomegaly" syndrome in commercial egg laying hens. Can Vet J **32:**500-501.
38. **Liu B, Sun Y, Chen Y, Du T, Nan Y, Wang X, Li H, Huang B, Zhang G, Zhou EM, and Zhao Q.** 2017. Effect of housing arrangement on fecal-oral transmission of avian hepatitis E virus in chicken flocks. BMC Vet Res **13:**282.
39. **Bhella D.** 2015. The role of cellular adhesion molecules in virus attachment and entry. Philos Trans R Soc Lond B Biol Sci **370:**20140035.
40. **Edgar RC.** 2004. MUSCLE: multiple sequence alignment with high accuracy and high throughput. Nucleic Acids Res **32:**1792-1797.
41. **Behrendt P, Bremer B, Todt D, Brown RJ, Heim A, Manns MP, Steinmann E, and Wedemeyer H.** 2016. Hepatitis E Virus (HEV) ORF2 Antigen Levels Differentiate Between Acute and Chronic HEV Infection. J Infect Dis **214:**361-368.
42. **Montpellier C, Wychowski C, Sayed IM, Meunier JC, Saliou JM, Ankavay M, Bull A, Pillez A, Abravanel F, Helle F, Brochot E, Drobecq H, Farhat R, Aliouat-Denis CM, Haddad JG, Izopet J, Meuleman P, Goffard A, Dubuisson J, and Cocquerel L.** 2018. Hepatitis E Virus Lifecycle and Identification of 3 Forms of the ORF2 Capsid Protein. Gastroenterology **154:**211-223 e218.
43. **Yin X, Ying D, Lhomme S, Tang Z, Walker CM, Xia N, Zheng Z, and Feng Z.** 2018. Origin, antigenicity, and function of a secreted form of ORF2 in hepatitis E virus infection. Proc Natl Acad Sci U S A **115:**4773-4778.
44. **Gao B, Vavricka SR, Meier PJ, and Stieger B.** 2015. Differential cellular expression of organic anion transporting peptides OATP1A2 and OATP2B1 in the human retina and brain: implications for carrier-mediated transport of neuropeptides and neurosteriods in the CNS. Pflugers Archiv-European Journal of Physiology **467:**1481-1493.
45. **Gao B, Hagenbuch B, Kullak-Ublick GA, Benke D, Aguzzi A, and Meier PJ.** 2000. Organic anion-transporting polypeptides mediate transport of opioid peptides across blood-brain barrier. Journal of Pharmacology and Experimental Therapeutics **294:**73-79.
46. **Shi R, Soomro MH, She R, Yang Y, Wang T, Wu Q, Li H, and Hao W.** 2016. Evidence of Hepatitis E virus breaking through the blood-brain barrier and replicating in the central nervous system. Journal of Viral Hepatitis **23:**930-939.
47. **Matsuda T, and Cepko CL.** 2004. Electroporation and RNA interference in the rodent retina in vivo and in vitro. Proc Natl Acad Sci U S A **101:**16-22.
48. **Choidas A, Jungbluth A, Sechi A, Murphy J, Ullrich A, and Marriott G.** 1998. The suitability and application of a GFP-actin fusion protein for long-term imaging of the organization and dynamics of the cytoskeleton in mammalian cells. European

Journal of Cell Biology **77:**81-90.

49. **Krogh A, Larsson B, von Heijne G, and Sonnhammer EL.** 2001. Predicting transmembrane protein topology with a hidden Markov model: application to complete genomes. J Mol Biol **305:**567-580.
50. **Chen YY, Liu BY, Sun Y, Li HX, Du TF, Nan YC, Hiscox JA, Zhou EM, and Zhao Q.** 2018. Characterization of Three Novel Linear Neutralizing B-Cell Epitopes in the Capsid Protein of Swine Hepatitis E Virus. Journal of Virology **92**.
51. **Brosch M, Yu L, Hubbard T, and Choudhary J.** 2009. Accurate and sensitive peptide identification with Mascot Percolator. J Proteome Res **8:**3176-3181.
52. **The UniProt C.** 2017. UniProt: the universal protein knowledgebase. Nucleic Acids Res **45:**D158-D169.
53. **Hillier LW, Miller W, Birney E, Warren W, Hardison RC, Ponting CP, Bork P, Burt DW, Groenen MAM, Delany ME, Dodgson JB, Chinwalla AT, Cliften PF, Clifton SW, Delehaunty KD, Fronick C, Fulton RS, Graves TA, Kremitzki C, Layman D, Magrini V, McPherson JD, Miner TL, Minx P, Nash WE, Nhan MN, Nelson JO, Oddy LG, Pohl CS, Randall-Maher J, Smith SM, Wallis JW, Yang SP, Romanov MN, Rondelli CM, Paton B, Smith J, Morrice D, Daniels L, Tempest HG, Robertson L, Masabanda JS, Griffin DK, Vignal A, Fillon V, Jacobbson L, Kerje S, Andersson L, Crooijmans RPM, Aerts J, van der Poel JJ, Ellegren H, Caldwell RB, Hubbard SJ, Grafham DV, Kierzek AM, McLaren SR, Overton IM, Arakawa H, Beattie KJ, Bezzubov Y, Boardman PE, Bonfield JK, Croning MDR, Davies RM, Francis MD, Humphray SJ, Scott CE, Taylor RG, Tickle C, Brown WRA, Rogers J, Buerstedde JM, Wilson SA, Stubbs L, Ovcharenko I, Gordon L, Lucas S, Miller MM, Inoko H, Shiina T, Kaufman J, Salomonsen J, Skjoedt K, Wong GKS, Wang J, Liu B, Wang J, Yu J, Yang HM, Nefedov M, Koriabine M, deJong PJ, Goodstadt L, Webber C, Dickens NJ, Letunic I, Suyama M, Torrents D, von Mering C, et al.** 2004. Sequence and comparative analysis of the chicken genome provide unique perspectives on vertebrate evolution. Nature **432:**695-716.
54. **Zinchuk V, and Grossenbacher-Zinchuk O.** 2009. Recent advances in quantitative colocalization analysis: Focus on neuroscience. Progress in Histochemistry and Cytochemistry **44:**125-172.
55. **Zheng CW, Li ZS, Yang N, and Ning ZH.** 2014. Quantitative expression of candidate genes affecting eggshell color. Animal Science Journal **85:**506-510.
56. **Troxler S, Marek A, Prokofieva I, Bilic I, and Hess M.** 2011. TaqMan real-time reverse transcription-PCR assay for universal detection and quantification of avian hepatitis E virus from clinical samples in the presence of a heterologous internal control RNA. J Clin Microbiol **49:**1339-1346.
57. **Park SJ, Lee BW, Moon HW, Sung HW, Yoon BI, Meng XJ, and Kwon HM.** 2015. Construction of an infectious cDNA clone of genotype 1 avian hepatitis E virus: characterization of its pathogenicity in broiler breeders and demonstration of its utility in studying the role of the hypervariable region in virus replication. J Gen Virol **96:**1015-1026.
58. **Billam P, Pierson FW, Li W, LeRoith T, Duncan RB, and Meng XJ.** 2008. Development and validation of a negative-strand-specific reverse transcription-PCR assay for detection of a chicken strain of hepatitis E virus: Identification of nonliver replication sites. Journal of Clinical Microbiology **46:**2630-2634.
59. **Waterhouse A, Bertoni M, Bienert S, Studer G, Tauriello G, Gumienny R, Heer FT, de Beer TAP, Rempfer C, Bordoli L, Lepore R, and Schwede T.** 2018. SWISS-MODEL: homology modelling of protein structures and complexes. Nucleic Acids Res **46:**W296-W303.

902 60. **Pettersen EF, Goddard TD, Huang CC, Couch GS, Greenblatt DM, Meng EC, and Ferrin TE.** 2004. UCSF chimera - A visualization system for exploratory
903 research and analysis. Journal of Computational Chemistry **25:**1605-1612.
904 61. **Kelley LA, Mezulis S, Yates CM, Wass MN, and Sternberg MJE.** 2015. The
905 Phyre2 web portal for protein modeling, prediction and analysis. Nature Protocols
906 **10:**845-858.
907
908
909

910 **FIGURE LEGENDS**

911 **FIG 1 Designation, prediction, expression, and identification of soluble GST-ap237 in**
912 **bacteria.** (A) Amino acids alignments of genotype 3 human and avian HEV truncated capsid
913 protein. The alignments of capsid proteins from genotype 3 HEV and CaHEV isolates were
914 performed using the Clustal W module of the MegAlign program of Lasergene 7.1
915 (DNASTAR, Inc.). (B) 3D structure of the CaHEV capsid protein was predicted by SWISS-
916 MODEL and visualized by CHIMERA software. The backbone of ap237 (aa 313-549) is
917 indicated in green in the pentamer (left). The P domain (blue), M domain (dark blue), S
918 domain (purple), and proline-rich hinge (green) of the monomer were highlighted with
919 different colors. (C) SDS-PAGE of GST-ap237 protein produced in *E. coli* Transetta (DE3)
920 cells. (D) Western blot analysis of the expression of recombinant GST-ap237 using anti-GST
921 antibody and GST-tag expressed by empty vector pGEX-6P-1 was used as a negative control.
922 (E) Western blot analysis of the expression of recombinant GST-ap237 using 3E8 mAb. The
923 vertical lines in panels D and E indicate marker (M) images; the Western blot results were
924 taken separately and joined together.

925 **FIG 2 SDS-PAGE analysis of host proteins by GST pull-down assay with GST-ap237**
926 **and identification of OATP1A2 in chicken embryo hepatocytes (CEH).** (A) GST pull-
927 down assay. GST protein was used to exclude the proteins bind with GST tag, and GST or
928 GST-ap237 without incubation of chicken liver cells lysate was set as blank controls. The
929 eluted protein complex was resolved by 10% SDS-PAGE, followed by silver staining. Five
930 visible bands specifically pulled by the ap237 protein are indicated by red arrow. (B)
931 Immunofluorescence assay of OATP1A2 protein in CEH using murine anti-GST-1A2^{ecto} sera
932 and TIRTC-goat anti-mouse IgG. Bar, 25 μm. (C) Western blot analysis of OATP1A2 protein
933 using murine anti-GST-1A2^{ecto} sera and HRP-goat anti-mouse IgG. WCL, CEH whole cell
934 lysates; LMH, LMH cell lysates; Cytos, CEH cytosolic proteins; SMPs & MAPs, solubilized

935 membrane and membrane-associated proteins from CEH; MFs, CEH membrane fractions.

936 **FIG 3 Interaction and co-localization of avian HEV capsid protein and chicken**
937 **OATP1A2.** (A) Immunoprecipitation with Protein G-anti-HA mAb. HEK 293T cells were
938 co-transfected with the recombinant plasmids, and the cell lysates obtained at 48 hours post-
939 transfection were immunoprecipitation with anti-HA mAb. The cell lysate and Protein G-Ab-
940 Ag complexes were detected by Western blot analysis. (B) Immunoprecipitation with Protein
941 G-anti-Flag mAb. (C) Co-localization of OATP1A2 with ap237. HEK 293T cells were co-
942 transfected with recombinant plasmids and then cells were fixed and subjected to indirect
943 immunofluorescence using mouse anti-HA mAb and rabbit anti-Flag pAb. The nucleus is
944 indicated by DAPI (blue) staining in the images.

945 **FIG 4 Prediction for extracellular domains of chicken OATP1A2 protein.** The
946 transmembrane helices of chicken OATP1A2 was performed by TMHMM server v.2.0. (A) A
947 list of the location of the predicted transmembrane helices. (B) The posterior probabilities of
948 inside/outside/TM helix. (C) The amino acids sequence of $1A2^{ecto}$.

949 **FIG 5 OATP1A2 ectodomain directly interacts with ap237.** (A) OATP1A2 structure was
950 predicted using the Phyre2 web portal. (B) SDS-PAGE (left) and Western blot analysis (right)
951 of GST-$1A2^{ecto}$ produced in Transetta (DE3) *E. coli* cells. (C) SDS-PAGE analysis of the
952 expression of ap237 protein without any tag. The purified ap237 protein was treated with
953 loading buffer containing 2-mercapto-ethanol and boiled 10 min (lane 1), and treated with
954 loading buffer without 2-mercapto-ethanol (lane 2). (D) GST pull-down assay to test $1A2^{ecto}$
955 binding with ap237. Beads conjugated to GST (lane 1) or GST-$1A2^{ecto}$ (lane 3) were
956 incubated with ap237. The incubation of the beads conjugated to GST-$1A2^{ecto}$ with sp239
957 (lane 2) was used as a control. After washing, proteins eluted from beads were analyzed via
958 SDS-PAGE, and then detected by anti-GST antibodies and 3E8 mAb. (E) Detection of

chicken OATP1A2 binding with ap237 by indirect ELISA. Different concentrations of ap237 were coated on ELISA plates and separately incubated with different concentrations of GST or GST-1A2^{ecto}. The binding of proteins was detected by anti-GST antibodies. (F) Evaluation of OATP1A2 binding with different HEVs capsid proteins by indirect ELISA. The proteins ap237, sp239, r239, sar239, and ker239 (4 μg/well) were coated and incubated with GST or GST-1A2^{ecto}. PRRSV N protein was used as a negative control.

FIG 6 Identification of LMH$^{1A2\text{-}GFP}$ cell line and knockdown of OATP1A2 expression. (A) Immunofluorescence assay of OATP1A2-GFP protein expression in the LMH$^{1A2\text{-}GFP}$ cell line. The recombinant protein OATP1A2-GFP was detected using mouse anti-GST-1A2^{ecto} sera and TIRTC conjugated goat anti-mouse IgG. The nucleus is indicated by DAPI (blue) staining in the images. (B) The relative expression of OATP1A2 mRNA in LMH, LMH^{GFP}, LMH$^{1A2\text{-}GFP}$, DF-1, and CEH. The LMH cells were used to normalize the relative expression levels in other cells. (C) Subcellular localization of OATP1A2 in LMH$^{1A2\text{-}GFP}$ cell. The 5 × 10^6 LMH$^{1A2\text{-}GFP}$ cells (or LMH^{GFP} cells) were used to extract the membrane protein. Three products, including cytosolic proteins (Cytos), solubilized membrane and membrane-associated proteins (SMPs and MAPs), and membrane fractions (MFs) were subjected for Western blot analysis using the anti-GFP antibody. (D) The knockdown of OATP1A2 expression in LMH$^{1A2\text{-}GFP}$ cells. LMH$^{1A2\text{-}GFP}$ cells were transfected with three OATP1A2-specific siRNAs (si1A2-1, si1A2-2, si1A2-3) or a control small interfering RNA (siNCtrl). After transfection for 48 hours, the cells were collected and total RNAs were obtained to detect the expression of OATP1A2 RNA. Western blot was performed using rabbit anti-GFP antibodies. (E) qPCR and Western blot for detection of OATP1A2 expression in LMH$^{1A2\text{-}GFP}$ cells treated with different concentration of si1A2-1. Error bars indicate the standard errors of the means (SEM). * P<0.05, ** P<0.01, *** P<0.001, **** P<0.0001; ns, not significant.

FIG 7 High levels of OATP1A2 expression enhance ap237 binding to the LMH cell. (A)

984 Western blot analysis of ap237 binding to the cell lines of LMH, LMH^{GFP} and LMH^{1A2-}
985 ^{GFP} transfected with siNCtrl or si1A2-1. The binding of ap237 to the cells was analyzed by
986 Western blot using 3E8 mAb. (B) Flow cytometry analysis of ap237 binding to LMH,
987 LMH^{GFP}, and LMH$^{1A2-GFP}$ cells transfected with siNCtrl or si1A2-1. After incubation with
988 ap237, cells were dissociated with enzyme-free cell dissociation buffer and fixed with 4%
989 paraformaldehyde to use for the flow cytometry assay. The mAb 3E8 was used to detect
990 ap237.

991 **FIG 8 High expression levels of OATP1A2 enhance CaHEV attachment and infection of**
992 **LMH cells**. (A) Determination of CaHEV propagation in the CEH, LMH, LMH^{GFP} and
993 LMH^{1A2GFP} cells. The infected cells were collected and total RNA was extracted to detect the
994 negative-strand (up) and positive-strand (bottom) CaHEV ORF3 genes using TaqMan real-
995 time RT-PCR and negative-strand-specific RT-PCR, respectively. Presence and absence of
996 negative-strand CaHEV RNA are indicated by "+" and "-", respectively. CaHEV attachment
997 (B) and infection (C) assays of LMH, LMH$^{1A2-GFP}$, LMH^{GFP}, and LMH$^{1A2-GFP}$ cells treated
998 with siRNA cell lines were performed. CaHEV ORF3 RNA was detected by TaqMan real-
999 time RT-PCR. Error bars indicate the standard errors of the means (SEM). * $P<0.05$, **
1000 $P<0.01$, ***$P<0.001$, **** $P<0.0001$; ns, not significant.

1001 **FIG 9 Inhibition of avian HEV attachment and infection of LMH$^{1A2-GFP}$ and CEH cells.**
1002 (A) Cytotoxicity analysis of the substrates (or inhibitors) at their maximum working
1003 concentration (50 μM, 50 μM, 10 μM, and 10 μM for CDCA, SC, carvedilol, and imatinib,
1004 respectively) for LMH$^{1A2-GFP}$ cells. (B) Detection of mRNA and protein levels of OATP1A2
1005 expression in LMH$^{1A2-GFP}$ cells treated with different substrates or an inhibitor. Anti-GFP
1006 antibody was used to detect the OATP1A2 fusions for Western blot. (C) Inhibition of CaHEV
1007 attachment and infection of LMH$^{1A2-GFP}$ cells by the substrates or inhibitor. After pre-
1008 incubation with CDCA, SC, carvedilol, and imatinib, CaHEV attachment (left) and infection

(right) assays were evaluated in LMH$^{1A2\text{-}GFP}$ cells. CaHEV ORF3 RNA was quantified by TaqMan real-time RT-PCR. (D) Blocking CaHEV attachment (left) and infection (right) in LMH$^{1A2\text{-}GFP}$ cells by ap237. (E) The anti-GST-1A2^{ecto} mouse sera blocked CaHEV attachment (left) and infection (right) in LMH$^{1A2\text{-}GFP}$ cells. sp239 protein and negative serum were used as controls. CaHEV ORF3 RNA was quantified by TaqMan real-time RT-PCR. Error bars indicate the standard errors of the means (SEM). (F) Inhibition of CaHEV infection of CEH was evaluated using imatinib, ap237, and murine anti-GST-1A2^{ecto} along with the corresponding DMSO, sp239, and negative mouse sera. (* P<0.05, ** P<0.01, *** P<0.001, **** P<0.0001; ns, not significant).

FIG 10 Correlation of OATP1A2 expression and avian HEV infection *in vivo*. (A) Localization of OATP1A2 protein in chicken tissues detected by IHC assay. OATP1A2 protein in chicken liver (a to f), spinal cord (g to l), brain (m to o), kidney (p to r), and testis (s to u) was detected using mouse polyclonal antiserum against 1A2^{ecto}. Positive immunoreactive signals are indicated by arrowheads. PBS and mouse anti-GST serum and were used as negative controls. (B) The relative expression of OATP1A2 mRNA in chicken tissues. Chicken tissues (0.2 g) were homogenized in RNAiso Plus reagent and total RNA was extracted. The total RNA (2 µl) was used as template to perform qPCR for OATP1A2 mRNA. GAPDH gene was used as a reference gene. (C) CaHEV ORF3 RNA in infected chicken tissues and fecal samples were detected by TaqMan real-time RT-PCR and negative-strand CaHEV ORF3 gene by negative-strand specific RT-PCR. The y-axis shows the amount of CaHEV ORF3 RNA copies per gram of chicken tissue. Presence and absence of negative-strand CaHEV RNA are indicated by "+" and "-", respectively.

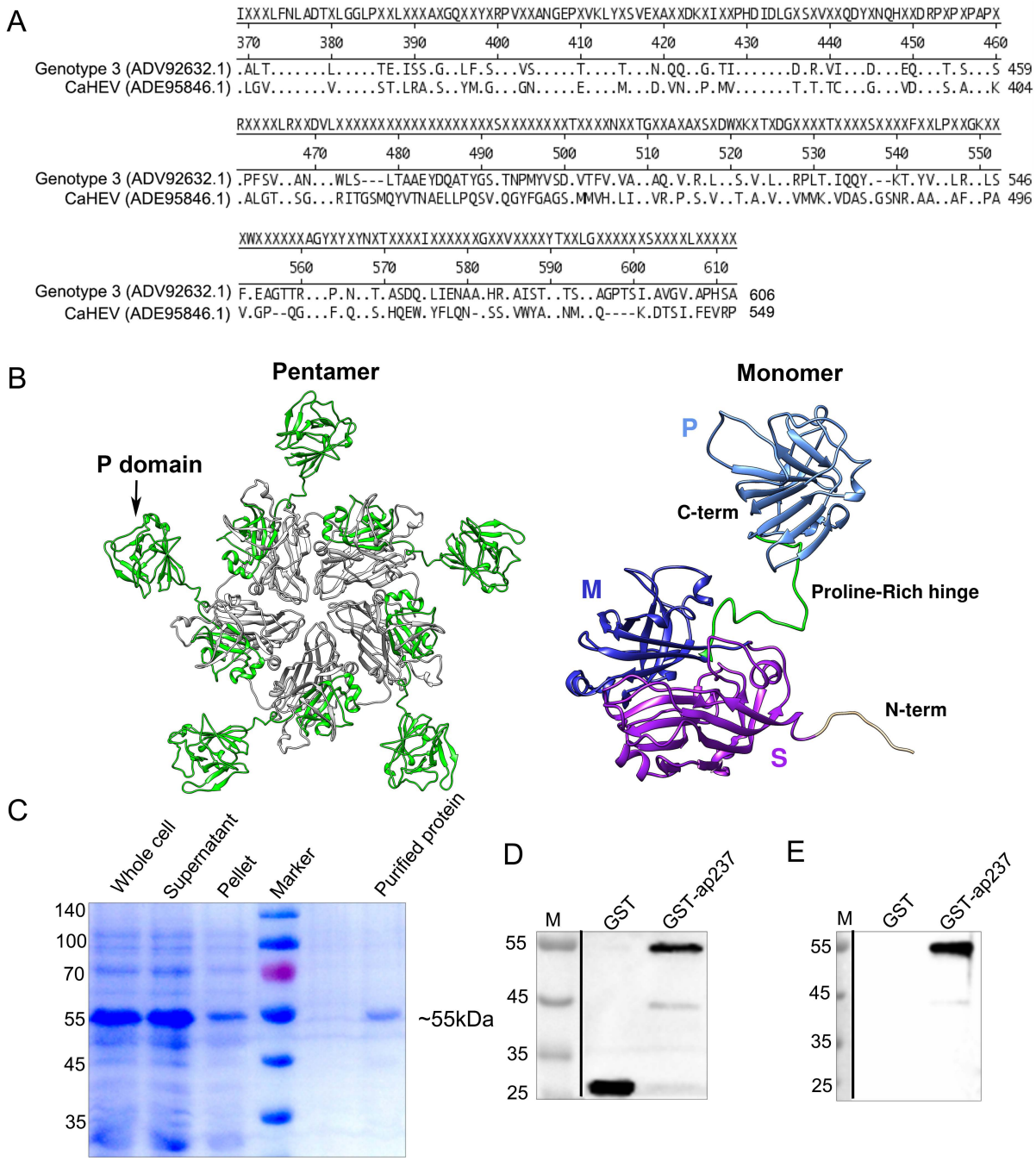

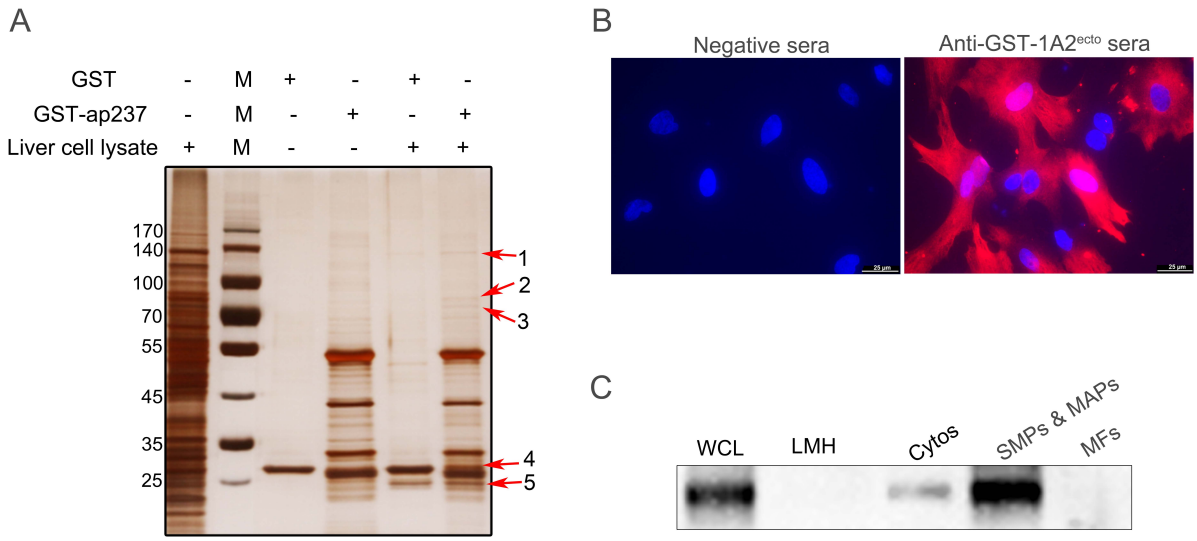

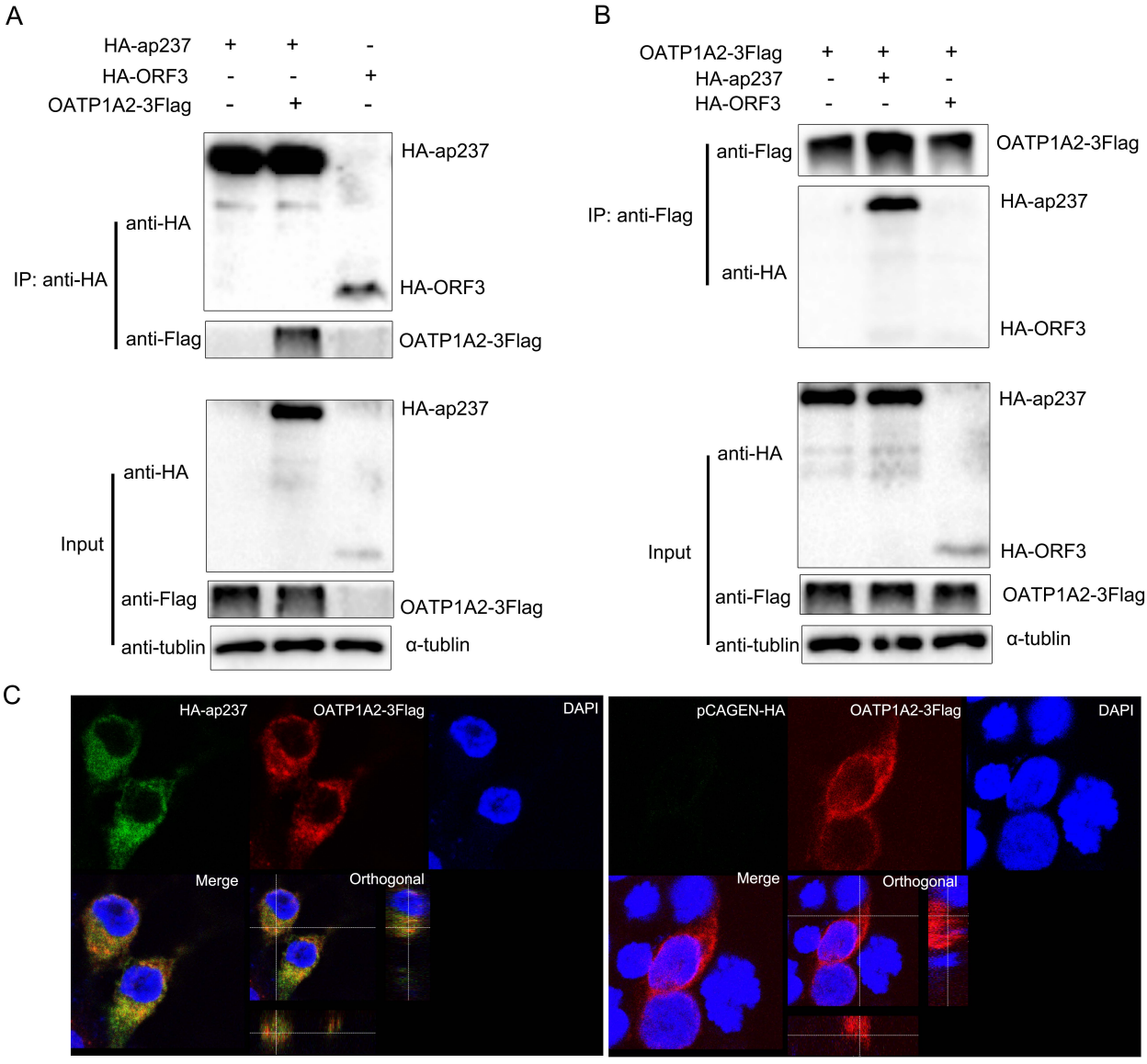

A

```
# 1 Length: 654
# 1 Number of predicted TMHs:  9
# 1 Exp number of AAs in TMHs: 240.56805
# 1 Exp number, first 60 AAs:  26.71953
# 1 Total prob of N-in:        0.97259
# 1 POSSIBLE N-term signal sequence
1        TMHMM2.0        inside       1     20
1        TMHMM2.0        TMhelix     21     43
1        TMHMM2.0        outside     44     52
1        TMHMM2.0        TMhelix     53     75
1        TMHMM2.0        inside      76     87
1        TMHMM2.0        TMhelix     88    110
1        TMHMM2.0        outside    111    243
1        TMHMM2.0        TMhelix    244    266
1        TMHMM2.0        inside     267    320
1        TMHMM2.0        TMhelix    321    343
1        TMHMM2.0        outside    344    357
1        TMHMM2.0        TMhelix    358    380
1        TMHMM2.0        inside     381    519
1        TMHMM2.0        TMhelix    520    542
1        TMHMM2.0        outside    543    556
1        TMHMM2.0        TMhelix    557    579
1        TMHMM2.0        inside     580    607
1        TMHMM2.0        TMhelix    608    630
1        TMHMM2.0        outside    631    654
```

B

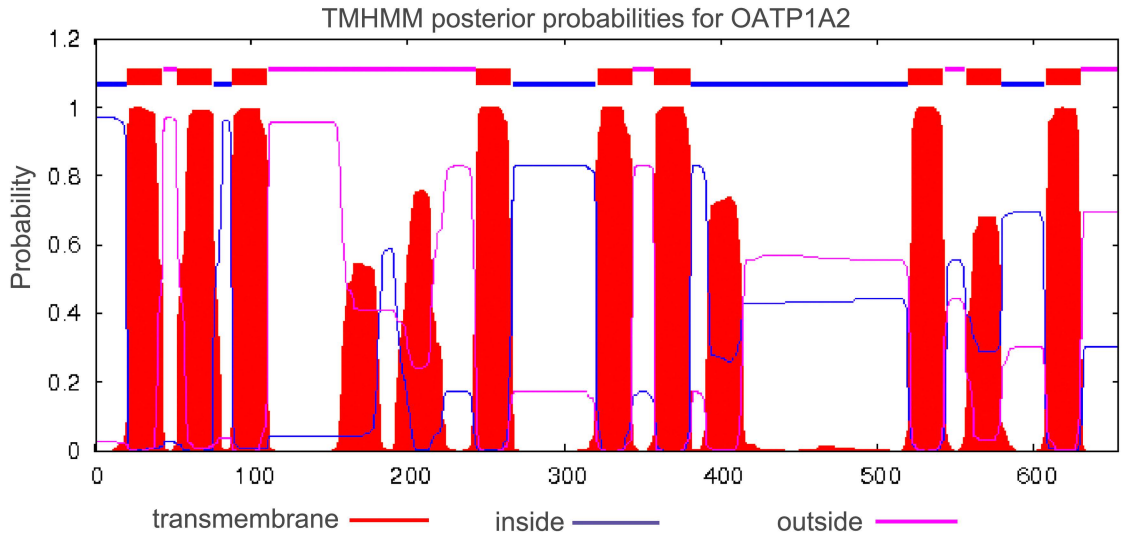

C

1A2^{ecto} sequence:

NSMYTQIEKQFNHFLFGRYHIES
SVSPQENSSVVSLCHANQSLTS
LPTEEPSTECEKEPESDLESVDA
GELTITPADVRWVGKYLEQQFG
KSASRSLKPEEKSFGKKKLKSER
NVSLNAPVELQDKGQ.

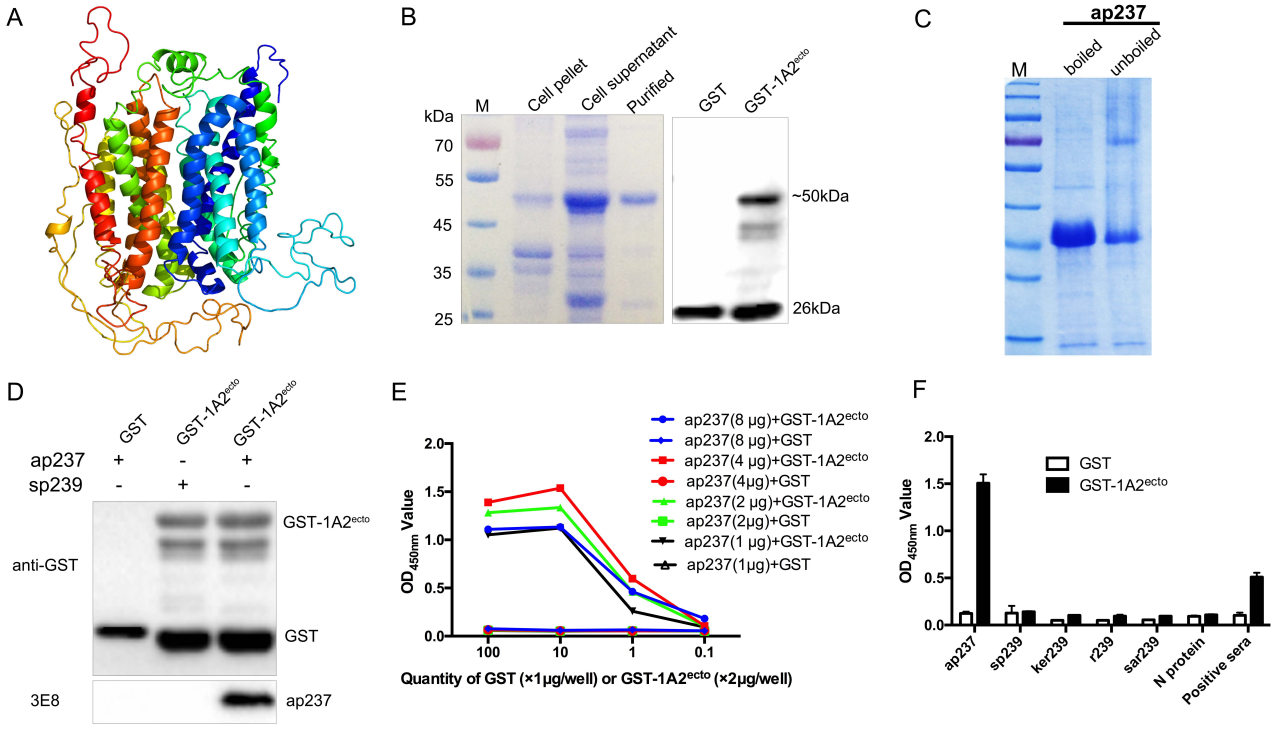

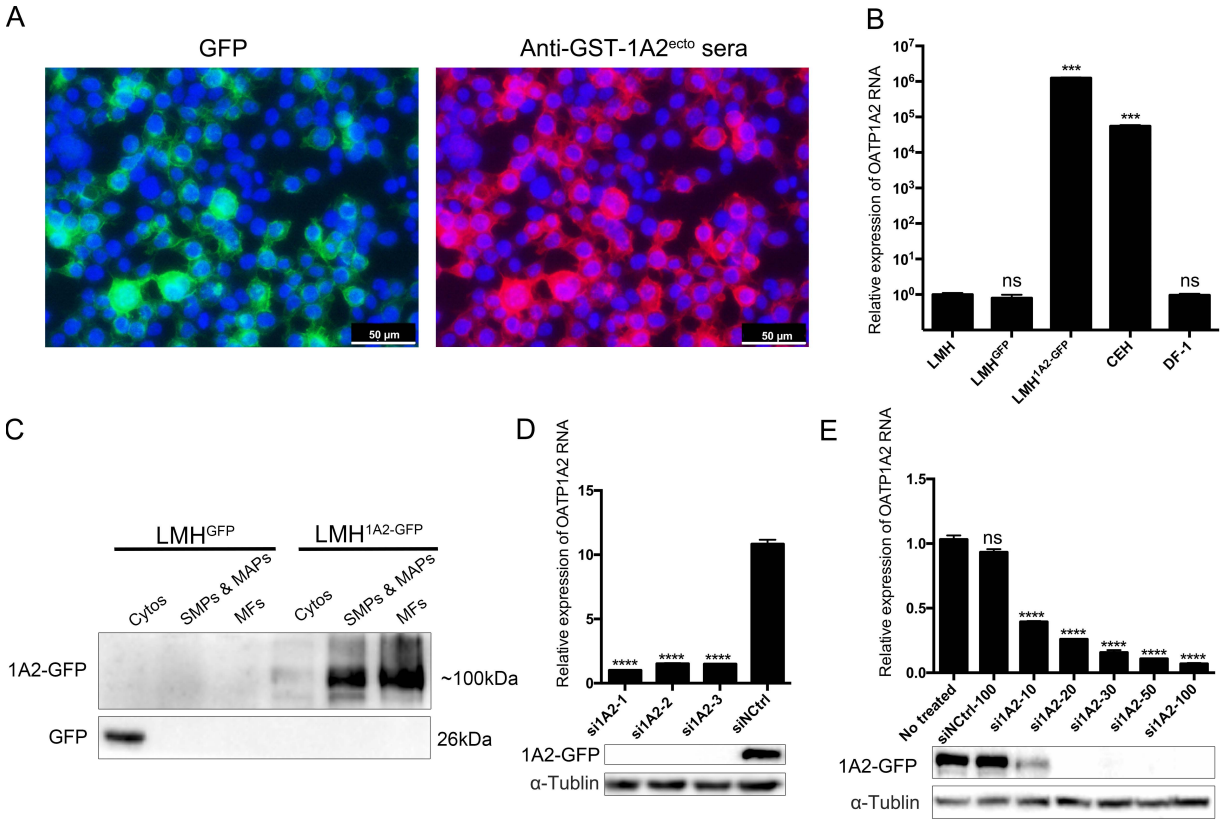

A

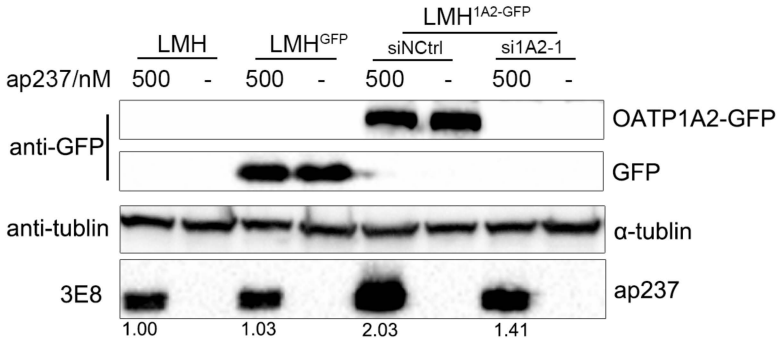

B

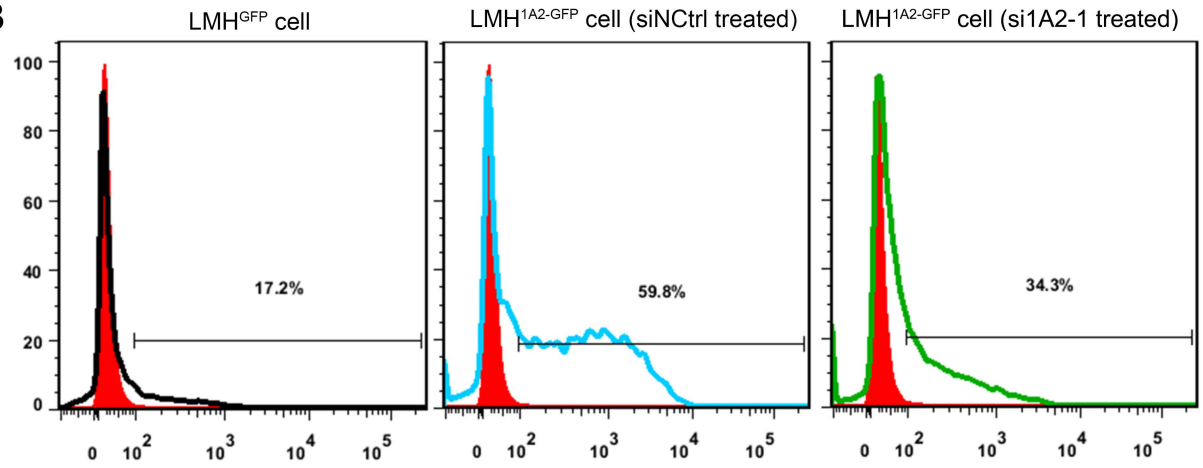

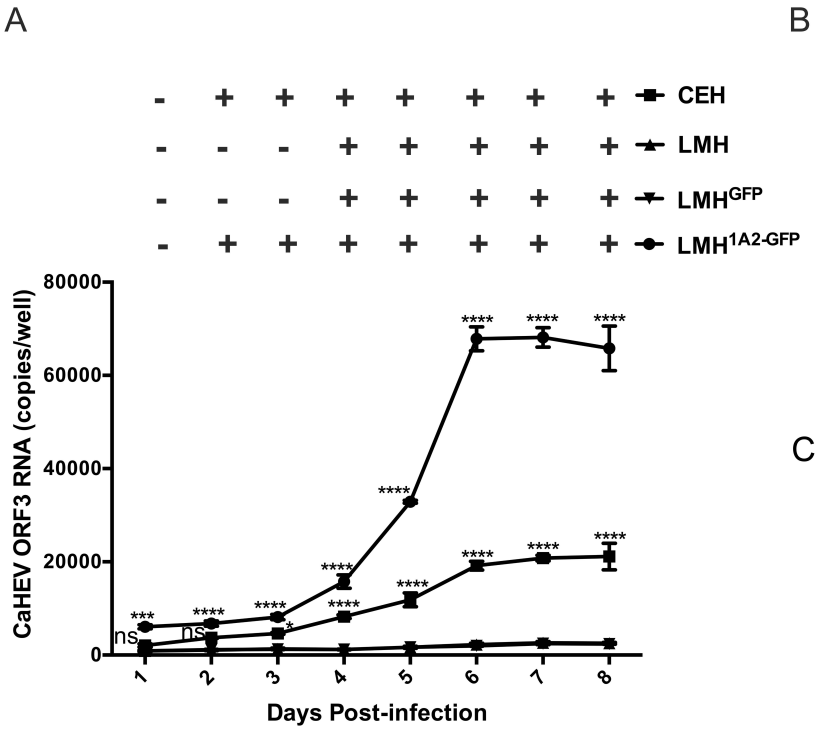

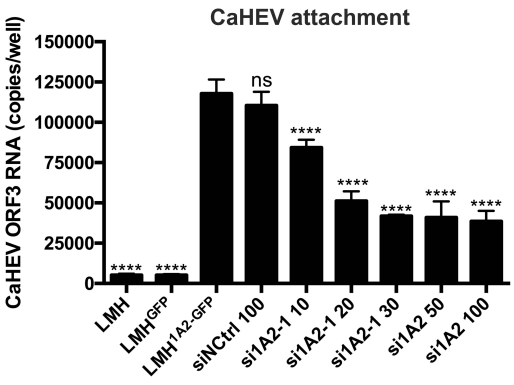

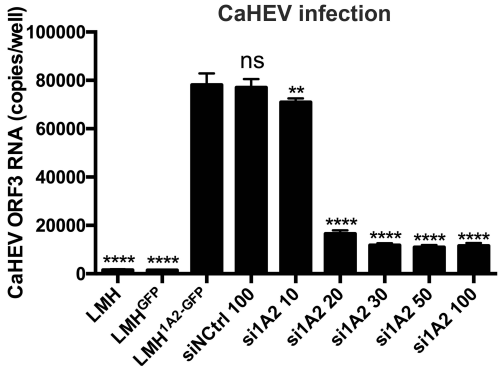

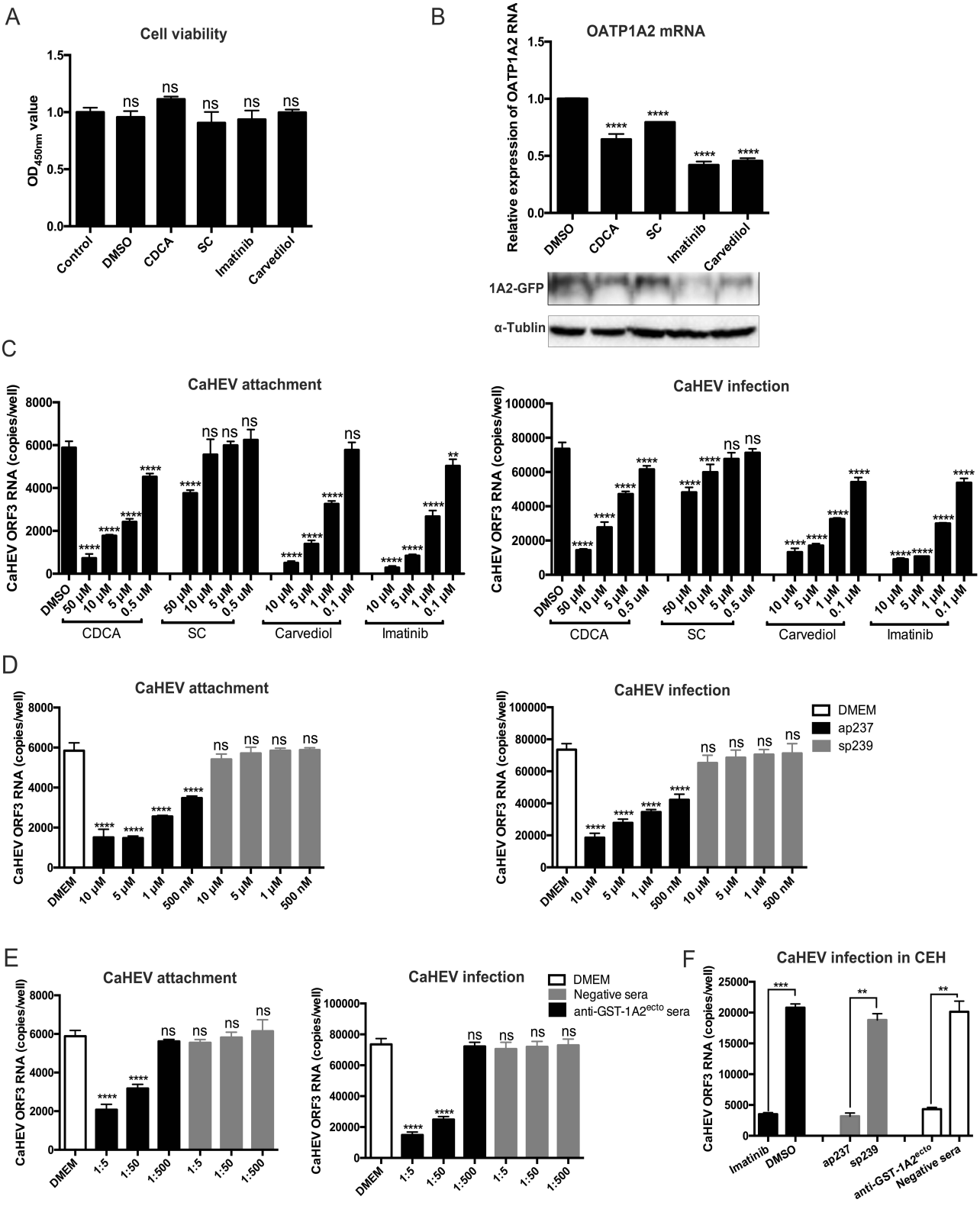

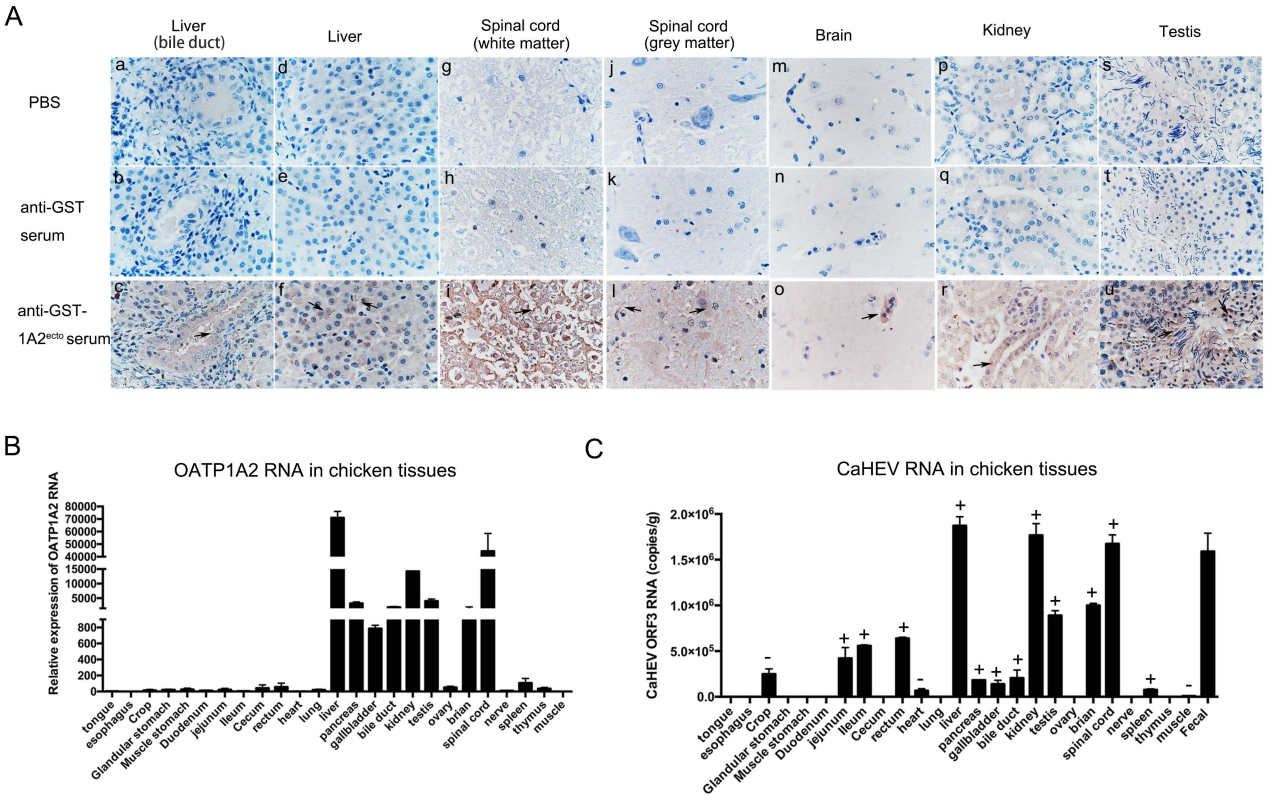

TABLE 1 Proteins present in five specific bands observed in the GST-ap237 lane of Fig. 2A as identified by MS

IDs/Uniprot	Protein name (short names, MW)	Sequence coverage [%]	Unique peptides	Locations
A0A1D5PMA0	Solute carrier organic anion transporter family member (OATP1A2, 72.542)	6.2	4	Cell membrane
P23668	16 kDa beta-galactoside-binding lectin (Galectin CG-16, 14.9)	23.88	3	Extracellular region or secreted
A0A1D5PDV6	Ribosomal protein S19 (RPS19, 15.4)	36.23	5	Nucleus
E1BRU7	Hexokinase domain containing 1 (HKDC1, 102.2)	27.32	4	Cytosol and Mitochondrion
F1N8M4	Dynamin-like 120 kDa protein, mitochondrial (OPA1, 113.3)	5.42	5	Mitochondrion
P84172	Elongation factor Tu, mitochondrial (TUFM, 38.3)	43.43		Mitochondrion
P0CG62	Polyubiquitin-B (UBB, 34.4)	44.59	3	Nucleus

TABLE 2 Primers used in this study

Primers	Sequence (5'-3') [a]
GST-ap237-F	CCGGATCCATCCTTGGCGTCTTGTTTAAT
GST-ap237-R	AAATCACTCGAGTGGCCGTACCTCGAAGAGGA
OATP1A2-F	GGAAGATCTATGAAAGAAACTCGGAAGC
OATP1A2-R	GGGTACCTTGTCCTTTATCCTGCAA
HA-ap237-F	CCGAGATCTATCCTTGGCGTCTTGTTTA
HA-ap237-R	CTAGGATCCTGGCCGTACCTCGAAGAG
Ap237-F	ATCCTTGGCGTCTTGTTTAAT
Ap237-R	TGGCCGTACCTCGAAGAG
1A2-F	GCTCTAGAATGAAAGAAACTCGGAA
1A2-linker-R	TTGAGCTCGAGATCTGAGTCCGGCCGGATTGTCCTTTATCCTGCAAT
Linker-GFP-F	AGATCTCGAGCTCAAGCTTCGAATTCAAAATGGTGAGCAA GGGCGA
GFP-R	CGGGATCCTTACTTGTACAGCTCGTCCA
GFP-F	GCTCTAGAATGGTGAGCAAGG
$1A2^{ecto}$-F	CGCGGATCCAACAGCATGTACACACAG
$1A2^{ecto}$-R	CCCTCGAGTTATTGTCCTTTATCCTGCAA
1A2-qF	GGCATTTCCAGGCTT AAGTTATTTC
1A2-qR	GCACCAGTCATCGTTTTACCAA
GAPDH-F	ATACACAGAGGACCAGGTTG
GAPDH-R	AAACTCATTGTCATACCAGG
Taqman-T7f	**TAATACGACTCACTATAGGG**TATGTGCTGCGGGGT
Taqman-F	TATGTGCTGCGGGGTGTCAA
Taqman-R	CATCTGGTACCGTGCGAGTA
EF1	ACGCAGGC GGAGTTTTGGTTGAGATTG
ER1	GAGTTAATTGGGCCAA TGTGGTGCCAG
EF2	TTGTTGGATATACCGCCGGCTCAT
ER2	TAATTACCGC AAGGCGGCTAGTGG

[a]The nucleotides of the linker sequence are underlined, and the T7 promoter sequence is in bold.